Investigating hydroclimatic impacts of the 168-158 BCE volcanic quartet and their relevance to the Nile River basin and Egyptian history

Ram Singh[1,2], Kostas Tsigaridis[1,2], Allegra N. LeGrande[2,1], Francis Ludlow[3], Joseph G Manning[4]

[1] Center for Climate Systems Research, Columbia University, New York
[2] NASA Goddard Institute for Space Studies, New York, NY-10025
[3] Department of History, School of Histories and Humanities, Trinity College, Dublin 2, Ireland
[4] Departments of History and Classics, Yale University, New Haven, CT 06520, USA

Correspondence to: Ram Singh (rs4068@columbia.edu)

Abstract.

The Ptolemaic era (305-30BCE) is an important period of Ancient Egyptian history known for its material and scientific advances, but also ongoing episodes of political and social unrest in the form of (sometimes widespread) revolts against the Ptolemaic elites. While the role of environmental pressures has long been overlooked in this period of Egyptian history, ice-core-based volcanic histories have identified the period as experiencing multiple notable eruptions, and a repeated temporal association between explosive volcanism and revolt has recently been noted. Here we analyze the global and regional (Nile River Basin) climate response to a unique historical case of 4 consecutive and closely timed large, strato-volcanic eruptions (first a tropical one, closely followed by 3 extratropical northern hemispheric events) between 168 and 158 BCE, a particularly troubled period in Ptolemaic history for which we now provide a more detailed hydroclimatic context. The NASA GISS ModelE2.1 Earth system model simulates a strong radiative response with a radiative forcing (top of atmosphere) of -7.5 W/m2 (following the first eruption) and -2.5 w/m2 (after each of the 3 remaining eruptions) at a global scale. Associated with this, we observe a global surface cooling of the order of 1.5˚C following the first (tropical) eruption, with the following three extratropical eruptions extending the cooling period for more than 15 years. Consequently, this series of eruptions constrained the northward migration of the inter-tropical convergence zone (ITCZ) during the northern hemisphere summer monsoon season, and major monsoon zones (African, South

Deleted: represents
Deleted: major
Deleted: ModelE
Deleted: Top
Deleted: 4.0
Deleted: at the surface

Asian, and East Asian) experienced a suppression of rainfall of >1 mm/day during the monsoon (JJAS) season averaged for 2 years after each eruption. A substantial suppression of the Indian and north African summer monsoon (over the Nile River headwater region) strongly affected the modelled river flow in the catchment and river discharge at river mouth. River mass flow over the basin was observed to consecutively decrease by up to more than 30% relative to an unperturbed (non-volcanic) annual mean flow for 2 years after the tropical eruption. A moderate decrease of up to 10-20% was observed after each of the remaining eruptions. These results indicate, in sum, that the first eruption likely produced a strong hydroclimate response, with the following 3 eruptions prolonging this condition. These results also support the recent hypothesized association between ice-core-based signals of explosive volcanism and hydroclimatic variability during the Ptolemaic era, including the suppression of the agriculturally critical Nile summer flooding.

Deleted: and Indian
Deleted: vigorously affects
Deleted: .
Deleted: decreases
Deleted: from volcanoes
Deleted: 15
Deleted: is produced
Deleted: show
Deleted: produces
Deleted: and
Deleted: prolonged the drying conditions.
Deleted: contention that the observed
Deleted: the
Deleted: impact of these eruptions
Deleted: Ptolemy
Deleted: for agriculture

Key Words: Volcanic eruption, hydroclimate impacts, Inter-tropical Convergence Zone (ITCZ), Monsoon, Nile River basin

1. Introduction

Large explosive volcanic eruptions that result in high altitude sulfate aerosol distribution across one or both hemispheres can diminish insolation, leading to both global and regional impacts on climate and society (e.g., Robock, 2000; Toohey et al., 2019). The sulfate aerosols resulting from (for example) the 1991 Mt. Pinatubo eruption of ~18 Tg SO_2 increased the optical depth of the atmosphere from ~0.6 to ~0.75 and was associated with surface cooling of 0.5 °C (Robock and Mao 1995; Parker et al., 1996). The cooling caused by such events can also reduce net evaporation and hence precipitation over large areas (Lui et al., 2016; Iles et al., 2013), while also potentially leading to a near global-scale dynamical suppression of the northward migration of the inter-tropical convergence zone (ITCZ) during the boreal summer, as the convergence follows the surface area of maximum temperature (Petterson et al., 2000; Chiang and Bitz, 2005; Broccoli et al., 2006; Colose et al., 2016). These changes in precipitation can, moreover, impact river outflow (Oman et al., 2006; Sabzevari et al., 2015; Kostiç et al., 2016), which has

Deleted: Stratovolcanic
Deleted: people (
Deleted: reduces
Deleted: (
Deleted: thus
Deleted: ;
Deleted: .
Deleted: boreal summer
Deleted:),
Deleted: .
Deleted:). Furthermore, these
Deleted: .

implications for civilizations from antiquity to the present-day, not least by affecting food security where agriculture is dependent upon this outflow. The Nile River, upon which Egyptian agriculture (and hence civilization) was heavily dependent, is a key example. With ice-core-based volcanic forcing histories now identifying several hundred potentially climatically effective eruptions over the past several millennia (Sigl et al., 2015), Egyptian civilization provides a valuable test-case for the study of human vulnerability and resilience to abrupt environmental change in potentially experiencing repeated "hydroclimatic shocks" induced by these events (e.g., Manning et al., 2017, 2021).

Explosive volcanic eruptions have become increasingly recognized as the major natural source of forced variability in the climate system at yearly to decadal time scales (Schmidt et al., 2011; Colose et al., 2016; Swingeduow et al., 2017; Khodri et al. 2017). Powerful explosive stratovolcanic eruptions can inject sulfur-rich gases high into the stratosphere, where they oxidize to form sulfate aerosol particles that can persist for months to years, in turn impacting the climate on regional to global scales. Volcanic aerosols in the stratosphere cause cooling in the troposphere by scattering incoming shortwave radiation, while also heating the stratosphere (Robock and Mao, 1992). Unequal north-south stratospheric heating due to volcanic aerosol presence concentrated in lower latitudes after tropical eruptions can influence major modes of atmospheric circulation and surface climate variability such as the Arctic Oscillation/North Annular Mode (AO/NAM) and North Atlantic Oscillation (NAO), in effect by driving an enhanced westerly airflow (Shindell et al., 2004; Zanchettin et al., 2021). The post-volcanic surface temperature response can also affect the El Niño/La Niña phase and Southern Oscillation, as well as having a long-term impact on Atlantic Meridional Overturning Circulation (AMOC) strength (Khodri et al., 2017; Wahl et al., 2014; Robock and Mao, 1995; Pausata et al., 2015). Extratropical eruptions are usually thought to have a comparatively weaker climate impact than tropical eruptions. This arises in part because of the background Brewer-Dobson circulation upwelling in the tropics and downwelling at higher latitudes, which directly affects the stratospheric lifetime of volcanic aerosols (Kirtman et al., 2013; Myhre et al., 2013; Schneider et al., 2009). Recent studies have, however, illustrated the potential for extratropical eruptions to dynamically include a disproportionally strong climate forcing (Toohey et al. 2019).

Volcanic injection of sulfur-containing compounds can, too, influence stratospheric chemistry, yielding further complex atmospheric and climatic responses upon interacting with water and halogens (LeGrande

Deleted: (Manning et al. 2017).

Deleted: no exception.

Deleted: hundreds of

Deleted: .

Deleted: may have been repeatedly influenced by

Deleted: wrought

Deleted: .

Deleted: are

Deleted: stratovolcanoes

et al., 2016; Brenna et al., 2020; Staunton-Sykes et al., 2021). Paleoclimate records and climate modeling efforts suggest that the dynamical response of volcanic aerosol causes a net (but regionally variable) drying effect and significantly impacts the global rainfall pattern (PagesHydro2k/Smerdon et al., 2017; Colose et al., 2016; Liu et al., 2016; Iles and Hegerl, 2014). For example, Trenberth and Dai (2007) analyzed the impact of the Pinatubo (1991) eruption on land precipitation and river streamflow and found an increase in associated drought conditions after the eruption in 1992. Joseph and Zeng (2011) suggested that varying responses to volcanically induced rainfall anomalies over land and ocean can seasonally modulate drought conditions in the tropics. In addition, hemispherical asymmetrical radiative forcing due to biases in the distribution of volcanic aerosols creates a radiative imbalance across the hemisphere, impacts the movement of ITCZ, constraining the extent of its summertime migration into the energetically deficit hemisphere (Colose et al., 2016; Xian and Miller, 2008). Effectively, the ITCZ shifts away from the hemisphere with the greatest amount of volcanic aerosol. For tropical eruptions, even those producing a roughly even hemispheric aerosol burden, this movement is typically more southward owing to the larger amount of land in the Northern Hemisphere and relative the greater ocean area (and higher thermal capacity) of the Southern Hemisphere.

For Africa, volcanic eruptions resulting in an asymmetrical latitudinal aerosol burden (e.g., the Katmai eruption in 1912 and El Chichón in 1982) are thus thought to have enhanced 20th century Sahelian drought conditions by shifting the surface temperature maxima and influencing the strength and position of Hadley cells (Haywood et al 2013). Of the Nile, monsoon rainfall over the Ethiopian highlands contributes (mainly via the Blue Nile and Atbara River) ~85% to the summer flood over the Egyptian plains and is a strong control over the associated interannual variability of the flood (Melesse et al., 2011). Years of diminished African monsoon rainfall were historically associated with insufficient river water to extensively practice the flood recession agriculture that ordinarily delivered such high agriculturally productivity in the Nile valley, and for which ancient Egypt was famed. But the Nile summer flood was also famously mercurial, with insufficient flooding often leading to adverse societal impacts (e.g., Bell, 1975; Butzer, 1976, 1984; Said, 1993; Hassan, 1997a, b; Hassan, 2007; McCormick, 2013). Some of this variability was likely driven by explosive volcanism. The Laki fissure eruption series (1783/84) thus injected approximately 122 Mt of SO_2 into the atmosphere over eight months and produced a strong

Deleted:)). Paleo

Deleted: Volcanic

Deleted: the

Moved (insertion) [1]

Deleted: The Laki fissure eruption series (1783/84) cooling and suppression of African monsoon (Oman et al., 2006; D'Arrigo et al., 2011), resulting in reduced Nile River flooding (Oman et al., 2005, 2006; Mikhail, 2015), or what is known colloquially as "Nile failure". Similar impacts have been simulated over the African region for the Katmai (1912) eruption (Vorosmarty et al., 1998; Thordarson and Self, 2003; Oman et al., 2005, 2006).

One of the most richly documented periods of ancient Egyptian history is the Ptolemaic era, 305-30 BCE, during which time Egypt was ruled by Greeks in a lineage beginning with Ptolemy I Soter (d. 283 BCE), who had been one of Alexander the Great's key generals and instrumental in the conquest of Egypt. The period distinguishes itself through its mixing of Greek and Egyptian traditions and its great material, cultural and scientific achievement (not least in the founding of the city of Alexandria on the Mediterranean coast with its famed Great Library and Lighthouse), but also through its chronic political instability (McGing, 1997; Ludlow and Manning, 2016; 2021). Little consideration has been given to external environmental influences in this history, despite the great dependence of Egyptian agriculture on the Nile summer flood. However, recent work has revealed a repeated close correlation between the timing and frequency of revolts and the ice-core-based dates of inferred-tropical and NH extratropical explosive eruptions (Ludlow and Manning, 2016, 2021; Manning et al., 2017). Just one example is the "Great Theban Revolt" of c.207 BCE, occurring shortly after a notable 209 BCE tropical eruption, when the Ptolemies lost control of large areas of the Nile Valley to a sequence of two apparently native Egyptian Pharaohs (Sigl et al., 2015; Ludlow and Manning, 2016; Ludlow et al., 2022).

The temporal correspondence between internal revolts and explosive volcanism certainly appears recurrent and non-random in the Ptolemaic Egypt (Ludlow and Manning, 2016, 2021; Manning et al., 2017; Izdebski et al., 2022). That the revolts and volcanic eruptions under study are known from different archives with independent chronologies (historical documentary and ice-core) has also helped to exclude potential biases in estimating this statistical significance. For example, inflated positive correlations may result when events are known from the same sources (e.g., between extreme weather and societal stresses such as famine or disease, if those instances of extreme weather that contributed to such stresses were more likely to have been documented than those that didn't (White and Pei, 2020)). While the results of Ludlow and Manning (2016, 2021) and Manning et al. (2017) thus implies a causal linkage between explosive eruptions and Ptolemaic-era revolts, much work remains to determine its underlying character,

Deleted: ,

Deleted: were

Moved up [1]: summer flood over the Egyptian plains and is a strong control over the associated interannual variability of the flood (Melesse et al., 2011).

Deleted: 2005; Oman et al., 2006). African monsoon rainfall over the Ethiopian highlands contributes (mainly via the Blue Nile and Atbara River) ~85% to the Nile

Deleted: Before the construction of large dams in the twentieth century, a failure of the African monsoon was thus historically associated with insufficient water to extensively practice the flood recession agriculture that ordinarily delivered such high agriculturally productivity in the Nile valley, and for which ancient Egypt was famed, often leading to adverse societal impacts (e.g., Butzer, 1976; Hassan, 1997; Hassan et al., 2007).

Deleted: through time (

Deleted: Historical records attest to dynastic power struggles and repeated revolts against Ptolemaic rule that have, until recently, been mainly credited to the poor quality of Ptolemaic leadership, particularly following the death of Ptolemy III in 222 BCE (McGing, 1997; Veïsse, 2004).

Deleted: Recent chronological corrections to ice-core-based volcanic forcing histories for the Ptolemaic period (Sigl et al., 2015) have, however,

Deleted: correspondence

Formatted: Font: Italic

Formatted: Emphasis, Font: 10 pt, Font color: Custom Color(RGB(14,16,26)), English (UK)

Formatted: Emphasis, Font: 10 pt, Font color: Custom Color(RGB(14,16,26)), English (UK)

Formatted: Emphasis, Font: 10 pt, Font color: Custom Color(RGB(14,16,26)), English (UK)

Formatted: Emphasis, Font: 10 pt, Font color: Custom Color(RGB(14,16,26)), English (UK)

Deleted: 2017), implying a previously unrecognized role for volcanism in the turbulent history of the kingdom. An

Deleted: Here

including how direct or indirect it may have been, whether this changed meaningfully between revolts (which varied in date, geography and scale), and (relatedly) what pathways were in effect to "operationalize" any such linkage. Answering such questions is now deemed a key challenge for climate historians and related scholars (White and Pei, 2020). Taken alone, such a correlation does not establish (nor necessarily even imply) causation. Causality is, however, at least implied in cases where analyses are conducted alongside statistical significance testing, with the resulting correlations considered unlikely to have arisen purely by chance, and when such results are interpreted with reference to the relevant historical context, allowing causal "pathways" to be credibly hypothesized (Izdebski et al., 2022).

For Ptolemaic Egypt, the fundamental hypothesized linkage involves the societal responses to sudden pronounced changes in hydrological cycle wrought by the widespread northern hemispheric cooling that can follow major explosive volcanic eruptions, and which can act (as noted above) to diminish net precipitation by reducing evaporation, as well as reducing the meridional (north-south) temperature contrast that controls the intensity of the African monsoon, alongside other regional factors. When this leads to a "failure" of the agriculturally critical Nile summer flood, a range of societal impacts may occur. These most obviously include agricultural and economic impacts (as can be seen in many periods of Egyptian history (e.g., Hassan, 1997a,b; Mikhail, 2015)), with reduced food security for families who may also have been less able to meet state taxation demands, potentially necessitating the sale of their hereditary lands and prompting migration from rural areas to larger urban areas in search of food (Manning, 2003; Manning et al., 2017). This would likely compound the psychological, religious and, ultimately, political significance of a "failed" Nile flood, with such an event being widely feared among the general populace and with the potential to be interpreted (and propagandized) as a reflection of divine displeasure at the Pharoah (Ludlow and Manning, 2021; Ludlow et al., 2022). In the context of the Ptolemaic period when parts of the populace, including at least some of the older native Egyptian elites and priesthood, were likely resentful of Greek rule and the taxation and other advantages given to those of Greek backgrounds (McGing, 1997; Ludlow et al., 2022), a Nile failure may have held additional political potency, offering further pathways by which volcanically induced hydroclimatic variability might motivate revolt onset.

Deleted: response

Deleted: hydroclimatic shocks

Deleted: reduce

Deleted: drives

Deleted: can be expected,

Deleted: ,

Deleted: a

Deleted: helping to explain the repeated link between ice-core-based eruption dates and major

Huhtamaa et al. (2022) have called for detailed case studies of both the hydroclimatic and socioeconomic impacts of specific volcanic eruptions to advance our understandings of human-environmental causalities. For Ptolemaic Egypt, the 160s BCE are thus of particular relevance in experiencing considerable internal revolt and instability. Indeed, the Ptolemaic dynasty might well have fallen here if not for self-interested Roman intervention against the Seleukid empire (great rivals to the Ptolemies), after their successful invasion (170-168 BCE) of Egypt under the command of Antiochus IV (Grainger, 2010; Blouin, 2014; Manning et al., 2017; see section S1.1 for additional historical context). This is also a decade remarkable for three notable volcanic eruptions (168, 164 and 161 BCE), with a further event in 158 BCE (Sigl et al., 2015). The distribution of sulfate across both poles (Sigl et al., 2015) identifies the first eruption (168 BCE) as the largest and likely occurring in the tropics, followed by three equally separated and comparably moderate-sized extratropical eruptions in the northern hemisphere.

While high-resolution palaeoenvironmental proxies for Egypt are effectively absent in this early period, our understanding of the hydroclimatic impacts of the sequence of eruptions between 168 and 158 BCE can be advanced by climate modeling. No previous study has specifically explored such a set of four closely consecutive eruptions or their impacts on the regional hydroclimate of a major ancient-era civilization. The few previous studies that have thus far examined the climatic and societal effects of eruption clusters include an exploration of the volcanic event cluster of the early 12th century (between 1108 and 1110 CE) (Guillet et al., 2020), the double event of the 6th century in 536 and 540 CE (Toohey et al., 2016), perhaps better seen as a triple event, in view of the additional, if much smaller, eruption in 546 (Sigl et al., 2015), and the eruption cluster from 1637 to 1641 (Stoffel et al., 2022; Huhtamaa et al., 2022). These studies have variously employed palaeoclimatic data, written evidence and/or climate model simulation to reveal the strong negative temperature anomalies over the Northern hemisphere following these eruptions, thereby suggesting the potential for adverse effects on crop yields and providing a climatic context by which to better understand the human history of these periods (Guillet et al. 2020; Toohey et al. 2016; Stoffel et al., 2022).

In this study, our main intent is to advance our understanding of the likely hydroclimatic impact of his eruption quartet as a foundation for further work aimed at establishing the nature of the causality underlying the observed association between volcanic eruptions and Ptolemaic-era internal revolts. We

Deleted: Important questions remain, however, in particular on the role of hydroclimatic shocks in the longer-term declining stability of the state and its ability to project power across the eastern Mediterranean. Repeated revolt in the third to first centuries BCE speaks to persistent vulnerability, yet despite experiencing the hydroclimatic effects of multiple eruptions (including those with a greater climate forcing potential than has been experienced in the twentieth and twenty-first centuries (Sigl et al., 2015)) and multiple such revolts, the dynasty persisted for almost three centuries, simultaneously suggesting a considerable level of resilience. It is conspicuous, however, that the dynasty ultimately ended (with Cleopatra's defeat by Rome at the naval battle of Actium in 31 BCE and her suicide in 30 BCE) in a decade that followed one of the largest explosive eruptions of the last 2,500 years in terms of climate forcing potential (based upon polar ice-core sulfate deposition levels), that of Okmok (Alaska) in early 43 BCE (McConnell et al., 2020). This itself followed a smaller but notable (likely extratropical NH eruption) in 46 BCE (McConnell et al., 2020). Egypt in the 40s BCE had, perhaps unsurprisingly therefore, experienced repeated Nile failure, famine, plague, inflation, administrative corruption, rural depopulation, migration, and land abandonment (Hölbl, 2001; Roller, 2010). It is notable though that there is no convincingly documented revolt, perhaps owing to Cleopatra's abilities as a leader and interventions in grain distribution to prevent starvation of the population. The stresses of the 40s BCE may still, however, be credibly posited as weakening Egypt's hand against Rome as it became entangled in the complex political and military developments of this major moment in world history, as Rome transitioned from its republic to imperial form (Manning et al., 2017; McConnell et al., 2020; Ludlow and Manning, 2021). ¶
Here clearly, as at any other time, the societal impact of a given hydroclimatic shock will be mediated by the prevailing historical context, but this does not mean all hydroclimatic shocks are of equal potential impact. Thus, regarding the association between explosive volcanism and Chinese dynastic collapse over the Common Era, the societal efficacy of volcanic climate forcing was observed to depend not only on levels of pre-existing or contemporaneous societal stress or instability (i.e., the historical context), but also on the magnitude of the climate forcing itself (Gao et al., 2021). Ice-core data suggest that the sequence of approximately 24 tropical and extratropical NH eruptions experienced by Ptolemaic Egypt varied in their climate forcing potential and were not distributed evenly in time (Sigl et al., 2015; Manning et al., 2017). Clusters of historical eruptions have at other times been examined for their potentially severe climatic and societal impacts (e.g., Toohey et al., 2016; Guillet et al., 2020; Campbell and Ludlow, 2020; Stoffel et al., 2022) and such an investigation can make a meaningful contribution to our understanding of the role of explosive volcanism in the history of Ptolemaic Egypt. A time of particular intertest is the 160s BCE, a decade of considerable internal revolt and instability. Indeed

Deleted: 2017).

Moved down [2]: ¶
While high-resolution palaeoenvironmental proxies for Egypt are effectively absent in this early period, our understanding of the hydroclimatic impacts of the sequence of eruptions between 168 and 158 BCE can be advanced by climate modeling.

Deleted:

Moved (insertion) [2]

Deleted: In this study, we

thus use a computationally expensive but more sophisticated version of the National Aeronautics and Space Administration (NASA), Goddard Institute for Space Studies (GISS) Earth system model, GISS ModelE2.1-MATRIX (Bauer et al 2008; Bauer et al, 2020), to simulate the series of eruptions from 168 to 158 BCE and analyze the impacts on regional hydroclimate over the Nile River basin. Details of the model and methodology employed to conduct the experiment and analysis are discussed in section 2. Our estimation of the background climate of the 2.5k (orbital and greenhouse gases (GHGs) changes only), together with the impacts due to PMIP4 vegetations are considered under section 3. Further subsections here evaluate the NASA GISS ModelE for its modelling capability in resolving the microphysical properties of volcanic aerosols during this period and analyze the radiative impacts of the aerosols arising from this eruption, which control the radiative and the hydroclimatic impacts of volcanic eruptions (Timmreck et al 2009; Timmreck et al., 2010; Schmidt et al. 2010). Finally, the discussion and conclusion (section 4) summarizes our results and considers how they can advance our understanding of the period's fraught human history in Egypt. This case of 4 closely consecutive eruptions presents a unique case to study the role of multiple eruptions on regional climate over such a critical region (Nile Basin).

2. Methodology & Experiment design

2.1 Model Description

We used the NINT (Non-INTeractive) version (Kelley et al., 2020) of GISS ModelE2.1 to simulate the background climate conditions corresponding to the period 2500 years before present (2.5ka, kilo-years BP), similar to the protocols developed for the mid-Holocene (6ka) coordinated experiment (Kageyama et al, 2017), except with trace gases and orbital forcing adjusted for 2.5ka. The term "non-interactive" means that atmospheric composition and climate are decoupled, so any changes in composition are handled by external input only. Once model attained an equilibrium climate state, we enabled atmospheric composition-climate interactions for the experiments performed here, as described below.

GISS ModelE2.1 is a state-of-the-art Earth System Model contributing to the Climate Model Intercomparison Project (CMIP) phase 6 (Eyring et al., 2016). The atmospheric component of GISS ModelE2.1 simulates on a horizontal resolution of 2° latitude by 2.5° longitude with 40 vertical layers

Deleted: ModelE,

Deleted: GISS ModelE2.1-MATRIX is the version of ModelE that has interactive chemistry and aerosol microphysics (MATRIX; Bauer et al., 2008, Bauer et al., 2020).

Deleted: analysed and discussed in

Deleted: , sub-sections under the section 3 also focus on the evaluating

Deleted: simulated volcanic aerosol properties

Deleted: analyzed

Deleted: volcanic

Deleted: due to

Deleted: set of 4 eruptions. These results focus on analyzing the modelling capability to resolve the microphysical properties of volcanic aerosols, aerosol optical depth and evaluation of aerosol size…

Deleted: controls

Deleted: climatic

Deleted: Schmidt et al. 2010). This is important because enormous volcanic eruptions may not have comparatively more significant climate impacts due to higher collision, larger size and affected radiative feedback (

Deleted: In section3, we also focus on analyzing the hydroclimatic impacts of volcanic quartet over the Nile basin region.

Deleted: summarize the

Deleted: consider

Deleted: 2.5ka years BP. The term non-interactive

Deleted: After reaching

and a model top at 0.1 hPa. It is coupled to the GISS Ocean v1 model at horizontal resolution of 1° latitude by 1.25° longitude with 40 layers. The Demographic Global Vegetation Model (DGVM) is the Ent Terrestrial Biosphere Model (TBM) (Kiang, 2012; Kim et al., 2015) is used to implement the climate-controlling vegetation properties, including the satellite-driven (MODIS) plant functional types (PFTs) and monthly varying leaf area index (LAI) (Gao et al., 2008; Myneni et al., 2002). Tree heights come from Simard et al. (2011) and include an interactive carbon cycle (Ito et al., 2020). The MATRIX (Multiconfiguration Aerosol TRacker of mIXing state) aerosol microphysics module (Bauer et al., 2008; Bauer et al., 2020) is used in the coupled composition-climate runs described here to simulate the active volcanism and corresponding climate conditions. MATRIX is an aerosol microphysics scheme using the quadrature method of moments, representing new particle formation (Vehkamaki et al., 2002), aerosol-phase chemistry, condensational growth, coagulation and mixing state of aerosols (Bauer et al., 2013). MATRIX tracks 16 mixing states with 51 aerosol tracers and resolves mixtures of sulfate, nitrate, ammonium, aerosol water, black carbon, organic carbon, sea salt and mineral dust (Bauer et al., 2008). MATRIX includes the direct effect and the first indirect effect of aerosols on climate.

An approximate eruption location is crucial to accurately estimate volcanic climatic impacts (Toohey et al., 2016, Aquila et al., 2018 [https://acd-ext.gsfc.nasa.gov/Documents/NASA_reports/Docs/VolcanoWorkshopReport_v12.pdf]). The broad hemispheric position of the 168 to 158 BCE volcanic quartet is thus chosen (to begin) with reference to the bi-polar multi-ice-core sulphate deposition data of Sigl et al. (2015), which allows a discrimination between likely tropical (low-latitude) eruptions and those likely occurring in the extratropics of either hemisphere. Without any firm additional data (e.g., ice-core tephra or direct geologic evidence) indicative of a more precise location, however, the ultimate location must be selected more arbitrarily. The chosen locations of all eruptions are shown in Fig S3. We note, however, that the longitude of each eruption is not expected to play a major role as an uncertainty factor. The forcing potential of these four eruptions in terms of atmospheric SO_2 injection is also estimated using the Sigl et al. (2015) multi-ice-core record of sulfate deposition over Greenland and Antarctica, linearly scaled corresponding to Pinatubo eruption estimates of 18.5 Tg SO_2 (Wolfe and Hoblitt, 1996). The injection height is selected to match that of Pinatubo, in the absence of any further information.

Deleted: The tree

Deleted: the

Deleted: interactively

Deleted: ,

Moved (insertion) [3]

Moved (insertion) [4]

Moved (insertion) [5]

2.2 Experiment Design

A control simulation for the 2.5ka period is performed using the PMIP4 (Paleoclimate Model Intercomparison Project) phase 4 protocols for the mid-Holocene (6ka) experiment, altered for conditions appropriate to 2.5ka. These include altering the orbital forcing, greenhouse gases (CO_2: 279 ppm, N_2O: 266 ppb, and CH_4: 610 ppb), as well as the vegetation in Africa and high boreal Eurasia and North America (Otto-Bliesner et al., 2017). Ozone and aerosols are prescribed to non-anthropogenic conditions only – this change is distinct from the pre-industrial simulations that include a small amount of anthropogenic changes and attendant aerosol and atmospheric chemistry change. The orbital and greenhouse gas forcings for the 2.5ka period are expected to play a vital role in producing the correct equilibrium climate. We ran a control run with the NINT configuration for 1000 years to get the model in equilibrium, and then extended this for 100 years by adding the MATRIX version of ModelE2.1 to again achieve an equilibrium state for a 2.5ka period with composition-climate interactions enabled. Vegetation cover, LAI and vegetation height are prescribed corresponding to the piControl period climate. The lack of exact vegetation cover information for the relevant period prevents the GCMs that lack dynamic vegetation model from reproducing mid-Holocene warm Northern hemisphere summer and enhanced NH monsoons conditions (Tierney et al, 2017; Larrasoaña et al, 2013). However, the vegetation cover used here as defined by the PMIP4 protocol vegetation sensitivity experiment (Otto-Bliesner et al., 2017) for the mid-Holocene period shows an intense impact on North-African rainfall and explains the difference between simulated and reconstructed climate conditions (Braconnot et al., 1999; Pausata et al., 2016). To address this, we created a modified mid-Holocene boundary condition sensitivity vegetation map by linearly interpolating between Pre-Industrial vegetation and the Mid-Holocene vegetation sensitivity experiment (northern hemisphere high latitude tundra during the preindustrial is replaced by boreal forests and African vegetation altered with evergreen shrubs replacing all vegetation up to 25N and grasslands up through the Mediterranean Coast in 6ka (Otto-Bliesner et al, 2017).

Fig S1 (Supplementary information) shows the major vegetation plant function type (PFT) cover changes under the PMIP4 sensitivity vegetation protocols after linearly interpolating for the 2.5ka period.

Deleted: the

Deleted: .

Deleted: turned on

Deleted: unavailability

Deleted: restrains

Deleted: without

Deleted: to produce

Deleted: For

Deleted: using the following postulates and

Deleted: 6ka and

Deleted: (PI) for

Deleted: 2.5ka period.

Deleted: <#>Northern hemisphere high latitude tundra during the preindustrial is replaced by boreal forests in 6ka.
Sahara in the preindustrial is replaced by evergreen shrubs up to 25N and further north with savanna/steppe in 6ka.

Deleted: <#>PFTs

The 2.5k equilibrated simulation with MATRIX is then extended for 70 more years with a corrected dust tuning, a typical process when equilibrating the model on a new climate state, and further 130 years with the linearly interpolated PMIP4 vegetation described above (refer to table TS1 for details of control runs and annual global mean time series of surface air temperature and precipitation in Fig. S2). This run equilibrated very quickly and no further tuning was needed. We thus used the last 100 of the total 130 years of that equilibrated run as the base climate for our analysis. An ensemble of 10 members with active volcanic eruptions was simulated using a restart file every 10 years during the last 100 years of the control simulation corresponding to 2.5ka period as summarized in table TS1, following the same approach as performed for the CMIP6 ensemble simulations (Kelley et al., 2020). The starting timepoint for each ensemble member is shown by blue vertical lines in fig S2. Each ensemble member started on January 1st of the year 169 BCE and ran for 16 years, with each eruption happening on the 15th of June of the 2nd, 6th, 9th and 12th years modelled. Because the exact date of an eruption cannot be directly determined based upon ice-core sulphate deposition data, both because of possible uncertainties in the ice-core chronologies and because of variable time lags between eruptions and the atmospheric circulation of the resulting sulphate and its deposition in the polar ice, we selected a summer eruption date to investigate the impact on northern hemisphere monsoon and wintertime atmospheric circulation. We also note that the accuracy of our modelling will depend in part upon the accuracy of the ice-core-based volcanic forcing reconstruction being employed. Uncertainties in reconstructed forcing can arise, for example, because of variation in the deposition of sulphate across the polar regions for any given eruption. In this respect, it is important to note that the Sigl et al. (2015) volcanic forcing reconstruction employs several ice-cores from Antarctica and Greenland, but our results can be revisited as reconstructions become more reliable by incorporating larger numbers of ice-cores.

Table 1. Details of eruptions applied in this experiment, with each eruption happening on the 15th of June of the 2nd, 6th, 9th and 12th model years.

Deleted: ¶

Deleted: , so we

Deleted: to

Deleted: .

Moved up [3]: (Toohey et al., 2016, Aquila et al., 2018 [https://acd-ext.gsfc.nasa.gov/Documents/NASA_reports/Docs/VolcanoWorkshopReport_v12.pdf]).

Moved up [4]: is thus chosen (to begin) with reference to the bi-polar multi-ice-core sulphate deposition data of Sigl et al. (2015), which allows a discrimination between likely tropical (low-latitude) eruptions and those likely occurring in the extratropics of either hemisphere. Without any firm additional data (e.g., ice-core tephra

Moved up [5]: Without any firm additional data (e.g., ice-core tephra) indicative of a more

Deleted: The broad hemispheric position of the 168 to 158 BCE series of eruptions

Deleted:) indicative of a more precise location, however, the ultimate location is by necessity selected more arbitrarily. The forcing potential of these four eruptions in terms of SO_2 injected into the atmosphere is also estimated using the Sigl et al. (2015) multi-ice-cire

Eruption	Year (BCE)	Position	Eruption injection (SO_2)	Injection Height (km)
E1	168	Pinatubo (15.13, 120.35) (Tropical)	22.5 Tg	22-26
E2	164	Mt Laki, Iceland (64.03, -18.13 W) (NH)	6.5 Tg	22-26
E3	161	Mt Katmai, Alaska Peninsula (58.28, -154.95 W) (NH)	7.2 Tg	22-26
E4	158	Shiveluch, Kamchatka, Russia (56.39,161.21) (NH)	7.5 Tg	22-26

3. Results

3.1. 2.5ka control runs

We evaluated the 2.5ka control climate run for a precise background climate for investigating the hydroclimatic impacts of the volcanic quartet from 168-158 BCE.

3.1.1 2.5Ka GHG+ORB climate

We compared the 2.5ka equilibrium climate with only GHG, orbital, and non-anthropogenic forcing changes against a preindustrial (year 1850) control run to evaluate the impact of orbital and greenhouse gas changes alone on our base climate state. Surface air temperatures show globally minimal differences with a warming of northern hemisphere high latitudes due to the different orbital forcing for all the seasons (Fig 1). The implications of changes in orbital forcing for 2.5k are thus evident in the surface temperature but the northern hemisphere monsoon season (JJAS) and winter season (DJF) rainfall slightly decreases along the northern equatorial belt. This points to the limitation of the GISS model in not having an interactively dynamic vegetation component to reproduce the mid-Holocene wet African land cover

Deleted: and

Deleted: temperature shows no noticeable

Deleted: except

Deleted: The

(Harrison et al., 2015; Tiwari et al, 2022). Numerous studies have demonstrated that including both biogeophysical feedback processes and atmospheric dynamics helps in achieving the wet African conditions for mid-Holocene (Kutzbach et al., 1996; Claussen et al., 2003; Kutzbach and Liu., 1997; Hewitt and Mitchell, 1998). Using the PMIP4 vegetation over the northern hemisphere regions has been shown to provide a solution to a long-standing issue with CMIP3/CMIP5 models that fail to reproduce these wet African conditions for mid-Holocene (Harrison et al., 2015).

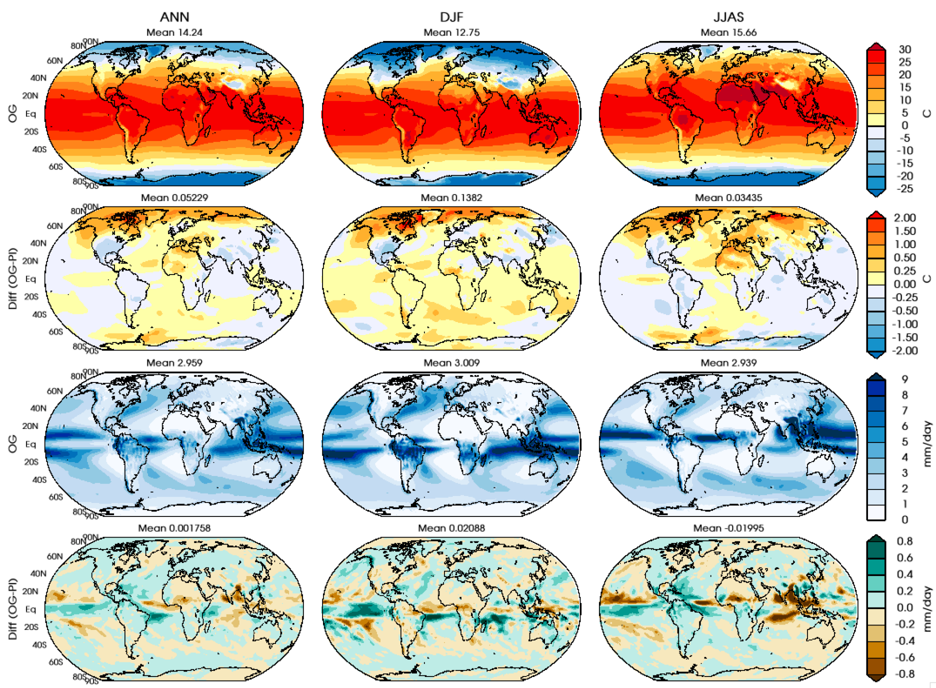

Fig 1. Seasonal means (Annual, DJF & JJAS) of surface air temperature (top row) for 2.5k period equilibrium run, differences from the preindustrial period (2.5ka-preindustrial) for all three seasons (2nd row from top) and seasonal (Annual, DJF & JJAS) mean precipitation (3rd row from top) and the

Deleted:).

Deleted: failing

Deleted:

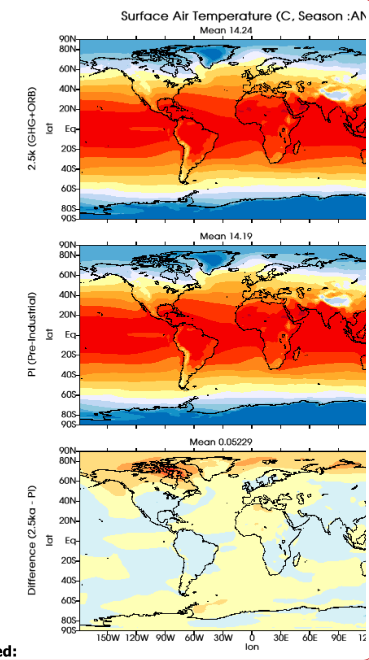

Deleted: mean

Deleted: left

Formatted: Line spacing: Multiple 1.15 li

Deleted: monsoon (

Deleted: season

Deleted: right) for the equilibrium runs with difference (bottom row) from preindustrial period (2.5ka-preindustrial). The equilibrium run for the 2.5k period include the orbital and GHG concentration changes for the 2.5k period (referred to as OG), the preindustrial period (as PI), and their difference (OG-PI) as simulated by GISS ModelE2.1.

3.1.2 2.5Ka ORB+GHG+VEG climate

The comparison of mean climate for the 2.5ka period for inclusion of PMIP4 vegetation is shown in fig 2 for the mean surface air temperature and precipitation for the Annual, DJF and northern hemisphere monsoon (JJAS) seasons.

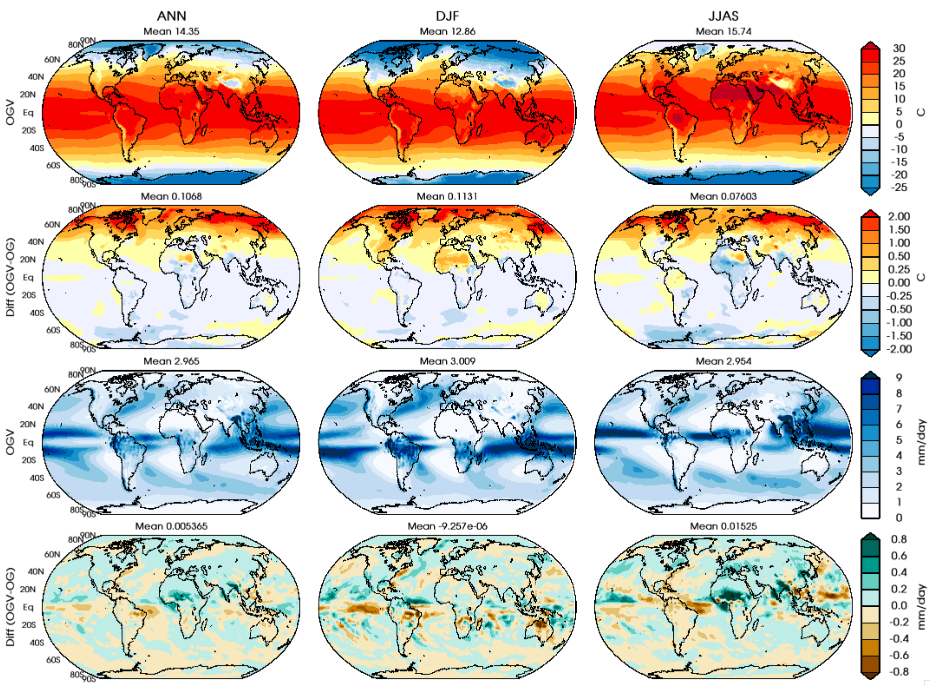

Fig 2. Mean surface air temperature for Annual, DJF and JJAS seasons (top row) and seasonal mean precipitation (3rd row from top) for the equilibrium runs with the PMIP4 vegetation for the 2.5k period and surface temperature difference (2nd row from top) as well as the seasonal precipitation differences

Deleted: only

Deleted: top

Deleted: middle

Deleted: 2.5ka-preindustrial; bottom

Deleted: annual

Deleted: season

Deleted:

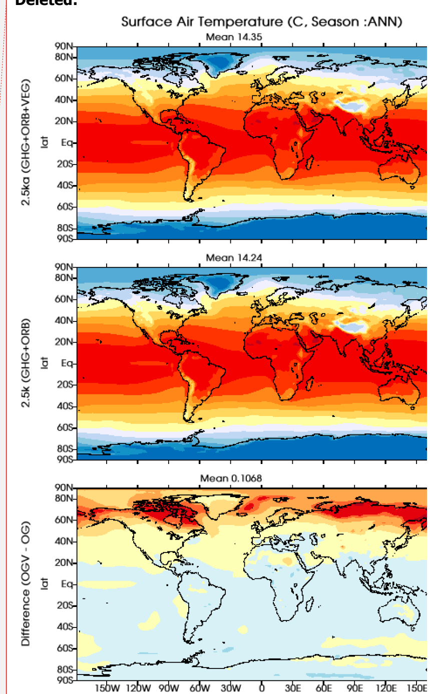

Deleted: Annual mean of

Deleted: (left)

Deleted: monsoon (

Deleted:) season

Deleted: right

Deleted: without (top row) and

Deleted: (middle row)

(bottom row) for the 2.5k period as simulated by GISS ModelE2.1. We used a short initial notation for forcing to denote the difference (ORB+GHG+VEG = OGV and ORB+GHG= OG)

GISS ModelE2.1 simulates a global a mean surface air temperature (SAT) of 14.4 ºC, 12.8 ºC and 15.7 ºC for Annual, DJF and JJAS seasons respectively for the 2.5ka (ORB+GHG+VEG) simulation, which is 0.11 C (Annual), 0.11 ºC (DJF) and 0.08 ºC (JJAS) higher than the 2.5ka (ORB+GHG) simulation without including these vegetation changes. A strong increase in the surface air temperature of greater than 2ºC is calculated over the northern hemisphere high latitude land regions, particularly in areas where land cover (tundra) is replaced by boreal forest, decreasing ground surface albedo during snowy winter months. A moderate rise of 0.5ºC over Africa is also simulated, which coincides with the regions of vegetation changes as described in section 2.2. The regional pattern of difference in rainfall in the northern hemisphere monsoon season (JJAS) is observed mostly over the North African and Asian regions. This observed increase of 0.4 mm/day or greater over the North African and Southwest Asian monsoon regions indicates a northward movement of the ITCZ during the monsoon season that is consistent with expectations given the modified vegetation for this period and is in agreement with our current understanding of mid-Holocene rainfall regimes (Tierney et al., 2017; Tiwari et al, 2022). These results also acknowledge the sensitivity of hydroclimatic impacts due to volcanic eruption to the regional land cover and hydrology alteration (Singh et al., 2020).

We also analyzed the zonal changes of longwave and shortwave radiation at the top of the atmosphere with our altered ground albedo, as shown in Fig 3. The vegetation-albedo feedback due to the inclusion of woody forest on higher latitudes and shrubs and steppes over northern Africa plays a crucial role in the additional monsoon season rainfall over the North African region. Greater vegetation cover for the Sahara and at higher latitudes in the Northern hemisphere alters the ground albedo by more than 10% regionally as well as altering the absorption of incoming solar radiations across the northern hemisphere higher latitudes (Fig 3). Consequently, it increases the pole-equator temperature gradient and pulls the ITCZ northwards as shown in Fig 2. It was thus concluded that the control climate generated using the PMIP4 vegetation scaled from the mid-Holocene to 2.5k period provides more precise and suitable control conditions to investigate the climatic impact of forcing perturbations due to volcanic eruptions. Vegetation boundary conditions implemented according to the PMIP4 sensitivity experiments with orbital and

Deleted: The difference of the two is shown at the bottom.

Deleted: annual

Deleted: the

Deleted: the order of 2-3 ºC

Deleted: , and a

Deleted: 5 ºC

Deleted: The

Deleted: suggests

Deleted: consistent

Deleted:).

Deleted: raises

Deleted: We

greenhouse gas forcing, helped to produce a precise equilibrium climate condition for this historically and climatically critical period 2.5ka years ago.

Deleted: help in producing

Deleted: important

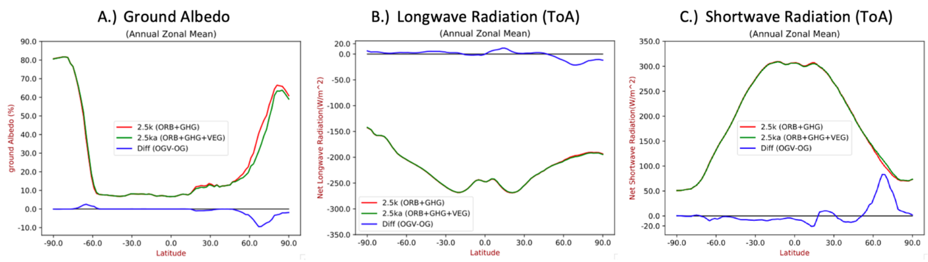

Fig 3. Annual zonal mean of ground albedo (A), longwave & shortwave radiation at the top of the atmosphere (ToA; B and C) for 2.5ka climates with ORB+GHG and ORB+GHG+VEG (red and green lines), respectively. The blue line shows the difference between them. The blue line in panel B & C is 10-fold (x10) to the original difference values in order to clearly show the difference on the same vertical axis.

Deleted: line)

3.2. Radiative forcing and climate response to volcanic aerosols

We simulate a series of four eruptions all occurring mid-June, during the 2nd, 6th, 9th and 12th years of the simulation, as described in section 2.2 and Table 1. Explosively injected SO_2 oxidizes to form aerosols in the stratosphere that can then alter the radiative balance at the top of the atmosphere by scattering incoming solar radiation and absorbing and re-emitting longwave radiation. Fig 4 shows the different components of the radiative budget on a monthly scale, with the annual cycle climatology removed for the entire period covering all four eruptions. The relative impacts of scattering the shortwave (SW) and absorbing the longwave (LW) radiation is proportional to the sulfate aerosol size (Lacis, 1992). The model simulated a lifetime for volcanically injected SO_2 as 31.4±0.72 days for eruption E1 and 24.4±0.44, 25.02±0.40 and 25.5±0.36 days for eruptions E2, E3 and E4, respectively. Other studies have reported a comparable average lifetime of 33 days (Read et al., 1993), 25±5 days (Guo et al., 2004), 35 and 25 days (Bluth et al., 1992; Schnetzler et al., 1995) for SO_2 injected from 1991 Pinatubo eruption using various satellite retrievals.

Deleted: forms

Deleted: 3

Deleted: eruption

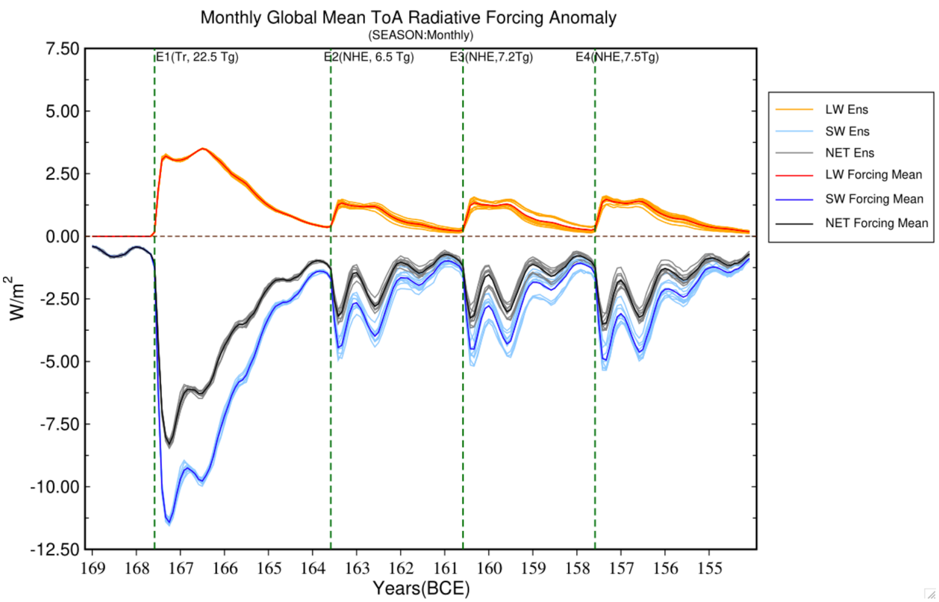

Fig 4: Monthly mean top of the atmosphere radiative balance perturbation due to volcanic aerosols for the entire simulation length. Orange/red shows the longwave radiative response, light/dark blue represents the shortwave, and grey/black represents the net (ToA) radiative change averaged at the global scale. The light-colored solid lines represent individual ensemble members, and the dark-colored lines show the ensemble mean. The green vertical dashed lines show when the eruptions happened.

With 22.5 Tg of SO_2 injected, the first, tropical eruption was larger than Pinatubo (~30%) and altered the longwave radiation budget by a mean of ~3 W/m^2 for almost a year after the eruption, while the other three eruptions were approximately 1/3rd of Pinatubo and produced a perturbation of the longwave radiative budget by ~1 W/m^2. The model simulates a strong impact on the shortwave radiation budget up to a mean of ~10 W/m^2 for a few months after the first eruption and of ~4 W/m^2 for a few months after each of the subsequent eruptions. A mean imbalance of up to -7.5 W/m^2 after the first eruption and -2.5-3 W/m^2 after the other eruptions in the top of atmosphere net radiative forcing suggests a strong

Deleted: 8

Deleted: suggest

corresponding surface cooling. Note that the bumps in the various radiative forcing trajectories apparent in Fig 5 in the year after each eruption reflect the seasonal cycle in the northern hemisphere. The presence of these volcanic aerosols in the atmosphere impacted climate in several keyways, as described below.

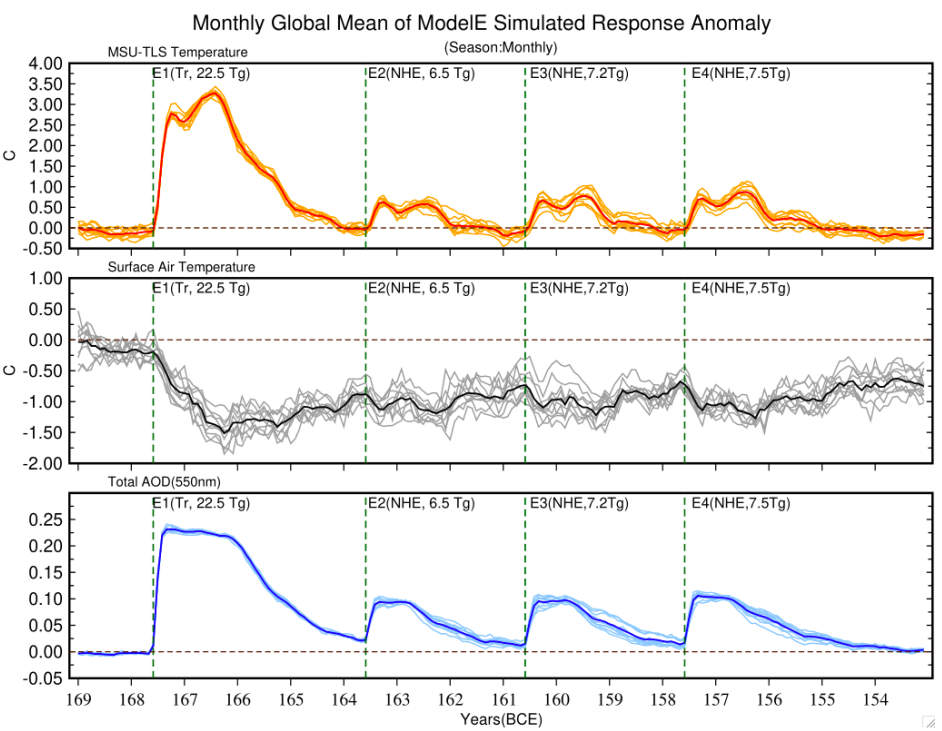

Fig 5. Globally averaged changes in MSU TLS (top panel), surface air temperature (middle panel) and total atmospheric column AOD at 550 nm for each month for the entire simulation period. The light-colored solid lines represent individual ensemble members, and the solid dark colors show the ensemble means. The green vertical dashed lines show when the eruptions happened.

Deleted: cooling at

Deleted: . The

Deleted: the eruptions

Deleted: of sun

Deleted: altered

Deleted: ways

The top panel in Fig. 5 shows the monthly change in microwave sounding unit (MSU) temperature for the lower stratosphere (TLS) as calculated by the model, which is a typical metric for present-day evaluation of modeled stratospheric temperatures against satellite data. It covers the lower stratosphere, where volcanic aerosols mostly lie, and represents the local atmospheric response of longwave absorption by them. After the Mount Pinatubo (1991) eruption, a lower stratospheric warming of the order of 2-3˚C for a year has been estimated using multiple reanalysis products (Labitzke and McCormick, 1992; Fujiwara et al., 2015). This is comparable to the ~25% larger eruption simulated here, E1, in which volcanic aerosols spread over a larger region (in both the northern and southern hemispheres) and absorbed a significant portion of longwave radiation, warming the lower stratosphere by up to 3ºC for the first two years after the eruption. This effect was seen to intensify during the second year, before starting to steadily decline in Years 3 and 4 with the scavenging of volcanic aerosols. The other three eruptions warmed the lower stratosphere by up to 0.5º C only, because these were both weaker and extratropical eruptions that only affected the northern hemisphere for a shorter period (~18 months).

The lower panel in Fig 5 presents the aerosol optical depth (AOD), a measure of atmospheric opacity to the incoming radiation as the extinction (sum of scattering and absorption) of shortwave radiation at 550nm. The model simulates an AOD anomaly of around 0.21 for the first 18 months after the first eruption, which decreases as aerosols are progressively removed. The subsequent eruptions produce an AOD of the order of ~0.1 which similarly decreases with time. For comparison, the AOD estimation for the Pinatubo (1991) eruption is 0.15 for approximately 12 months over a background optical depth of ~0.6 (Russell et al., 1996; English et al., 2013).

In the upper troposphere and lower stratosphere, the impact of each of these eruptions is distinct with a near-complete recovery to background AOD levels after each (i.e., and before the next) event; however, at surface, a lag in recovery time is evident (middle panel in Fig 5). The net impact of radiative flux perturbations following the eruptions is summarized in the form of the global surface air temperature change over the entire period. The model produces a robust mean cooling of ~1.5º C in the second year (or proceeding year) after the first eruption, and although AOD recovers a few years after each eruption, the surface temperature response is more prolonged. This lag in global mean surface air temperature response can be mainly ascribed to the thermal inertia of the oceans which need more time to return to

Deleted: is

Deleted: somewhat

Deleted: absorb

Deleted: intensifies

Deleted: warm

Deleted: The lag in global mean surface air temperature response (Middle panel) is mostly due to the thermal inertia of ocean which needs more time to return to the normal as shown in the supplementary information (Fig S4).

Deleted: being

Deleted: on

the normal. This sea surface temperature (SST) response is shown in fig S4, with a slower post-eruption recovery and remanent cooling effect. (as shown in the supplementary information (Fig S4)). The smaller extratropical eruptions (E2-E4) that followed the large tropical one (E1) are then observed to hinder the surface temperature recovery and maintain a surface cooling of around 1.0ºC during the entire period of simulation. Comparatively, the 1991 Mt. Pinatubo eruption created an ~0.5°C (peak) cooling over 1-2 years after the eruption (Hansen et al 1996).

Deleted: hindered

Deleted: maintained

Deleted: The sea surface temperature (SST) response shown in fig S4 suggest a slow recovery of the oceans

Deleted: eruptions with a remanent cooling effect.

3.3 Volcanic aerosol properties

The effect of volcanic aerosols on radiative forcing is tightly controlled by aerosol size (Lacis et al., 1992; Hansen et al., 1980). The aerosol effective radius, R_{eff}, is a key metric in linking aerosol microphysical properties with their SW and LW impacts. The vertical profile of aerosol size as represented by R_{eff} is calculated for each month and is shown in Fig 6. After the tropical eruption (E1), new aerosols nucleated and grew rapidly via coagulation and, while SO_2 was still available, by condensation, and attained a maximum R_{eff} of greater than 0.5 μm approximately for 2 years. In comparison, R_{eff} after the Pinatubo eruption went up to 0.6 μm and sustained that size for approximately 2 years (Russell et al., 1996). Sulfate aerosol sizes for the subsequent three smaller extratropical eruptions (E2 to E4) grew up to 0.3 μm.

Deleted: nucleate

Deleted: grow

Deleted: is

Deleted: attain

Deleted: grow

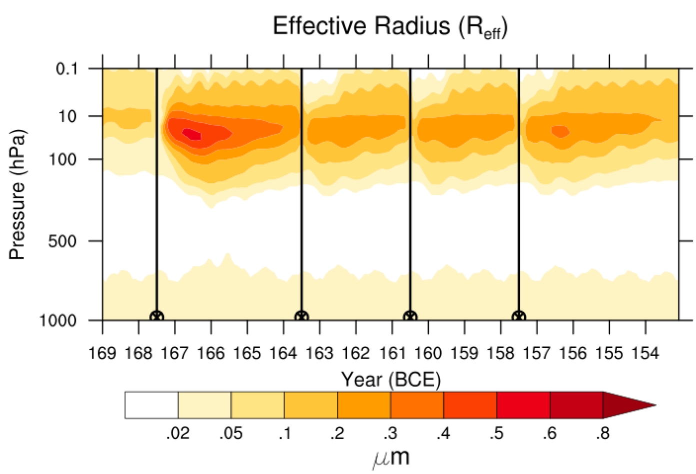

Fig 6. Timeseries of the global ensemble mean vertical profile of sulfate aerosol R_{eff} for the entire simulation period. The vertical black line with a circled cross mark on the horizontal axis shows the timing of the eruptions.

Deleted: at

Deleted: bottom

The aerosol extinction vertical profile (Fig S5A) shows that the radiative impact of the E1 tropical eruption in the lower stratosphere was prolonged as compared to the later extratropical eruptions. Heating of the lower stratosphere affects the dynamics of the stratosphere; after tropical eruptions enhanced tropical upwelling and extratropical downwelling with the phase of Brewer-Dobson circulation have an impact on the transportation of trace species such as Ozone (O_3) and NO_2 (Aquila et al., 2013; Trepte et al., 1992; Pitari et al., 2016; Pitari and Mancini, 2002). Fig S5B shows a strong positive (≥10 ppbv) anomaly of CH_4 in the upper stratosphere and negative (≤10 ppbv) anomalies in the lower stratosphere, especially after the tropical eruption (E1). Changes in the mean concentration of upper and lower stratospheric methane (CH_4) suggest a strong vertical transport (Kilian et al., 2020).

Deleted: is

3.4. Latitudinal temperature response to volcanic aerosol forcing

The Hovmöller diagram (Fig 7A and 7B) shows the differences between the zonally averaged AOD at 550nm and surface air temperature response for the ensemble means of the volcanic eruption simulations as compared to the mean climatology of the control simulation. The statistical significance level is estimated using the 2-tail student t-test after Deser et al., (2012) and following the assertion that 10 ensembles are sufficient for reasonable estimation of internal variability at a regional scale (Singh and AchutaRao, 2019). The pattern of total AOD after the first eruption (E1) shows a strong cross-equatorial transportation of the stratospheric aerosols into the southern hemisphere, with a similar pattern in the northern hemisphere. This is consistent with the hypothesis that an enhanced Brewer-Dobson circulation in the southern hemisphere during the austral winter season can lead to the southward transportation of volcanic aerosols after a Pinatubo type (tropical) eruption (Aquila et al. 2012). The initial dispersal of aerosols from eruption E1 was strongly influenced by its timing and exhibited a seasonal dependence (consistent with Toohey et al., 2011). However, the other three eruptions (E2, E3 and E4) in the high latitude extratropic only yielded an increased AOD in the northern hemisphere.

Deleted: difference of

Deleted: between

Deleted: mean

Deleted: led

Deleted: is

Deleted: exhibits

Deleted: are

Deleted: extratropics and

Deleted: yield

A lag of more than 12 months in the peak surface temperature response (Fig 5 Middle panel) after the first eruption correlates well with the distribution of aerosols, consistent with findings reported in the literature for similar events (e.g., Jungclaus et al., 2010; Klocke, 2011). The global mean surface temperature response peak thus appears when the volcanic aerosols from the tropical eruption (E1) have extended across the northern hemisphere extratropics and the polar regions. It should be noted that the land surface over the northern extratropics is observed to respond quickly to the attenuated post-eruption shortwave radiative flux compared to the tropics. The zonally averaged surface temperature response (fig 7B) shows that a strong cooling of 1.0-1.5˚C lasted over the tropical north and partially over the tropical southern hemisphere for more than 30 months after the first eruption. Further, the greater anomalies of >2.0 ˚C cooling mostly appeared six months after the first eruption, with the subsequent extratropical eruptions helping to maintain the northern hemispheric cooling.

Deleted: extend

Deleted: responds

Deleted: lasts

Deleted: appear

The seasonality of surface temperature response reveals a more substantial cooling during the boreal summer season for all four eruptions and for E1 also reveals the expected post-tropical-eruption winter warming pattern over Europe. Supplementary Fig S6 shows the spatial pattern of the surface temperature response to volcanic aerosols over the four seasons directly following the first eruption (E1) (JJA & SON for the year of eruption and DJF & MAM for the next year). The surface temperature response for the first two seasons is confined to the tropics and moves to higher latitudes after six months. As evident in fig S3, the anomalous winter (DJF) warming pattern after the eruption over Europe and an observed cooling over Northern America may be a product of the same fundamental atmospheric dynamics as noticed after Pinatubo eruption (Robock, 2000; Robock and Mao, 1992).

Deleted: after tropical eruptions (E1)

Deleted: the

Deleted: could

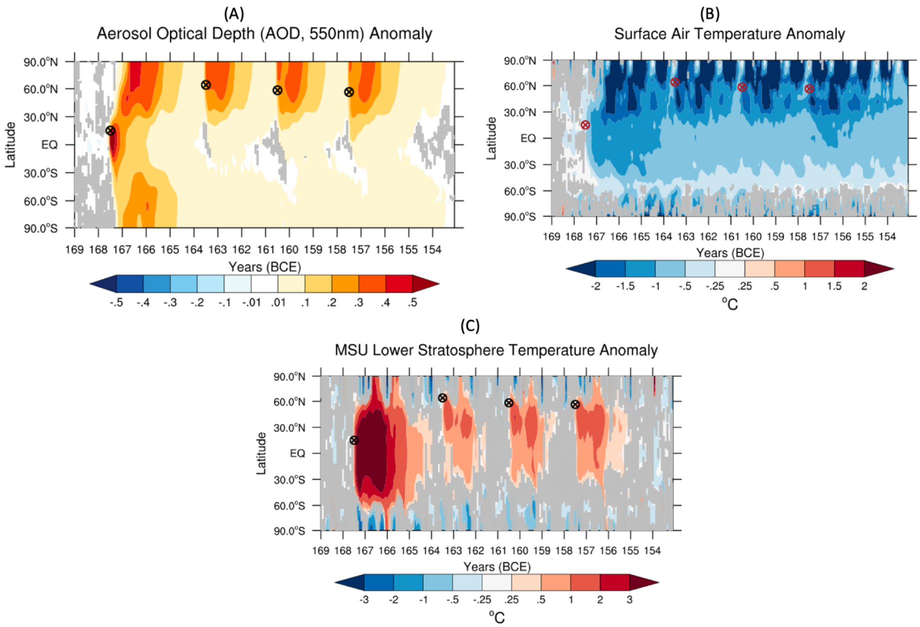

Fig 7. Hovmöller diagram showing the zonally averaged temporal dispersion of volcanic aerosols in terms of AOD change at 550nm (A), surface temperature response (B), and lower stratospheric temperature response (C). Anomalies were calculated with respect to a climatological annual cycle calculated from the control simulation. The gray color is painted over the regions where changes are not statistically significant at the 95% confidence level. Circled cross marks show the modeled spatial and temporal position of the eruptions.

The global lower stratospheric temperature response in terms of MSU TLS data has been discussed in section 3.2. Interestingly, fig 7C shows that the latitudinal anomaly of the lower stratosphere warming is broadly limited to the equatorial lower stratosphere. Eruption E1 induces lower stratosphere warming on the order of >3 °C, with a weaker warming of up to 1-2 °C after the three extratropical eruptions (E2, E3 and E4). Lower stratosphere warming also affects the polar vortex strength in the northern hemisphere

Deleted: is

and atmospheric circulations into the troposphere, with substantial repercussions for surface climate and variability patterns as suggested in previous research (e.g., Graf et al., 1993, 2007; Shindell et al., 2004).

3.5 Latitudinal precipitation response to volcanic aerosols

We used a coarser resolution earth system model having a simplified parameterization and successful in simulating the large-scale patterns of rainfall change (Kelley et al., 2020). Numerous studies using the observational record in addition to modeling efforts have demonstrated that the cascading impact of an altered radiative balance at the top of the atmosphere due to volcanic eruptions is reflected in the hydrological cycle in terms of regional patterns of seasonal rainfall change (e.g., Robock and Liu, 1994; Robock, 2000; Trenberth & Dai, 2006; Schneider et al., 2009, Iles et al., 2012; Iles and Hegerl, 2014; Timmreck, 2012). Societies conducting agriculture in arid and semi-arid regions before the advent of modern reservoirs and irrigation, such as in ancient Egypt, are perhaps most impacted by such changes. We thus investigate the hydrological cycle response to this set of eruptions at a global and regional scale, paying particular attention to the northern hemispherical monsoon season (JJAS) for the first 2 years following each eruption for the period under study. It can be argued that any individual ensemble member might best represent the historical period, but it is impossible to select the most accurate member in the absence of supporting observational data from period of interest. Also, the added noise due to natural variability can alter the sign of change at the spatial scale among the individual ensembles. Thus, we selected the mean across the ensemble and its statistical inference to show the response to volcanic eruptions with robustness for the specific climate variables under consideration. Fig 8 shows the Hovmöller diagram of the zonal mean precipitation anomaly relative to the annual cycle climatology of the 100-year-long control simulation.

Deleted: regard

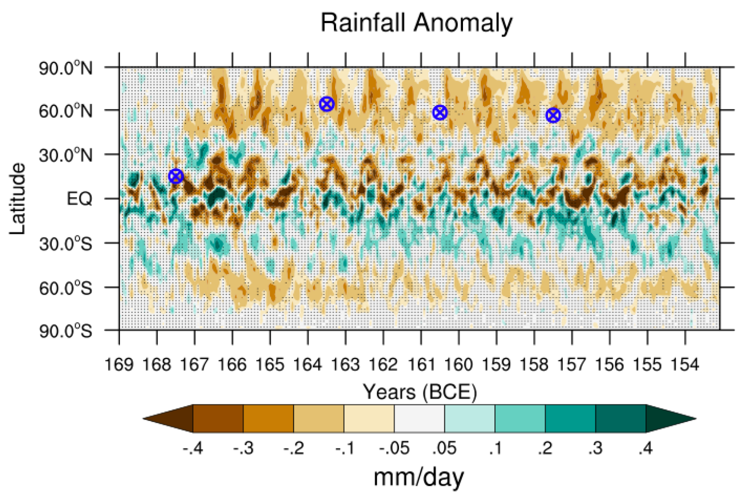

Fig 8. Hovmöller diagram showing the zonally averaged rainfall anomaly for the entire period as the spatiotemporal response of global rainfall to our series of volcanic eruptions. Circled cross marks show the locations and timing of the eruptions. Black dots point out the regions where changes are not statistically significant at the 95% confidence level.

The ensemble zonal mean rainfall change after the eruptions showed a substantial negative trend in the northern hemisphere as a result of cooling induced by the volcanic aerosols. A robust negative anomaly of the order of 0.3-0.4 mm/day in the northern hemisphere rain belt (ITCZ) region appeared shortly following the first eruption (E1) and persisted during the following couple of years (Fig 8). A pattern of strong drying in the equator also coincided with the northern hemisphere monsoon season (JJAS) for 2 to 3 years after the eruption (E1). However, because the rainfall response in the northern hemisphere extratropics strongly correlates with the surface temperature response, it was thus seen to emerge here 12 months after the tropical eruption (E1), with the model calculating a moderate to a high decrease on the order of 0.1-0.2 mm/day in rainfall, a response that persisted throughout the year for three post eruption years. A shift in the northern hemisphere rainfall pattern was also evident for the region around 30ºN, with slight increases in rainfall for 2 years after the tropical eruption (E1). This response was statistically

Deleted: shows
Deleted: due to
Deleted: appears after
Deleted: persists
Deleted: .
Deleted: coincides
Deleted:).
Deleted: and
Deleted: emerges
Deleted: persists
Deleted: is
Deleted: is

significant over only a few spots after the first eruption, however. Fig 8 clearly demonstrates that a drying pattern also prevailed after the later extratropical eruptions (E2-E4). Because of this the northern hemisphere experienced a sustained net (albeit temporally varying) precipitation decline for the entire modeled period, and with a distinct seasonal character.

Deleted: is
Deleted: evident
Deleted: other
Deleted:) and that because
Deleted: experiences

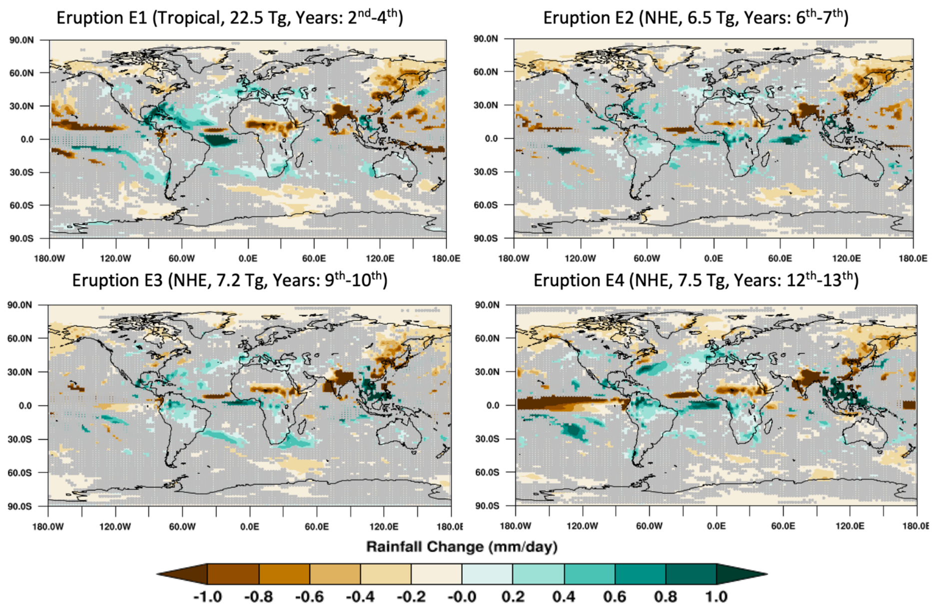

Fig 9. Mean change (mm/day) in northern hemisphere monsoon season (JJAS) rainfall averaged for three consecutive years after eruption E1 and two years after each of E2, E3 and E4 (left to right and top to bottom). The caption over each panel shows the eruption characteristics. A gray color is painted over the grid boxes for which change in rainfall is not significant at the 95% confidence level. Years indicated in parentheses follow the order of the eruptions in our simulation period, i.e., E1 occurs in the 2nd simulation year, and E2-E4 occur in the 6th, 9th and 12th years, respectively.

We further evaluated the spatial patterns of change in mean rainfall during the northern hemisphere monsoon season (JJAS) as shown in Fig 9. We averaged the three monsoon seasons (eruption year and next 2 years) after the more potent tropical eruption (E1) and two monsoon seasons (eruption year and next year) after each of the remaining extratropical eruptions (E2, E3 and E4), and focused principally on identifying statistically significant responses. Hence, after the tropical eruption, the summer monsoon rainfall appeared strongly suppressed over many major northern hemisphere monsoon regions. Importantly for our historical focus on Egypt, African monsoon rainfall showed a notable decrease of 0.5-1.0 mm/day during the three-year post-eruption JJAS season average (i.e., derived from the eruption year and first two post-eruption years). This decrease covered a large area in Africa from (approximately) the equator to (approximately) 17ºN. The South and East Asian monsoon regions were also shown to experience a robust negative rainfall anomaly of >1.0 mm/day over the Indian subcontinent as well as (more variably) several regions of China, though with some isolated increase over the eastern Vietnamese landmass. Similar patterns of decreased rainfall also appeared over the western (and particularly northwestern) Pacific and northern hemispheric high latitude regions more broadly. The model also simulated a (statistically significant) band of enhanced JJAS rainfall stretching from Central Asia westward through the Near East and into the Mediterranean (touching on parts of northern Africa), Western European and parts of the North Atlantic (roughly between a latitudinal band of 30ºN to 50ºN). A contiguous band of increased rainfall was also observed further south and west in the Atlantic, stretching into parts of the northern Caribbean, southeastern Gulf of Mexico and Mesoamerica (fig 9). Similar patterns of suppressed boreal monsoon season rainfall were observed following each of the extratropical eruptions (E2-E4), but a particularly notable east-west band over both land and ocean (broadly confined between slightly north of the equator and 30ºS) shows a positive rainfall anomaly (being most clearly statistically significant between (approximately) 5ºN and 10ºS (fig 9)). This pattern is largely consistent with past literature employing observations and modeling of volcanic climatic impacts under a range of scenarios and periods (e.g., Robock, 2000; Robock and Liu, 1994; Iles et al., 2012; Liu et al., 2016; Haywood et al., 2013; Schneider et al., 2009; Trenberth and Dai, 2007; Joseph and Zeng, 2011; Gu and Adler, 2011). In terms of mechanisms, for many northern hemisphere landmasses, these eruptions clearly induced a surface cooling that altered the northern hemisphere meridional

Deleted: fig
Deleted: appears
Deleted: shows
Deleted: which includes
Deleted:).
Deleted: covers
Deleted: are
Deleted: appear
Deleted: ,
Deleted: is
Deleted: portions
Deleted: are
Deleted: have
Deleted: has

(equator-to-pole) surface temperature gradient (fig 7). Given this energetic deficit, we may posit that the northern hemisphere (NH) experienced a post-eruption alteration of large-scale circulation patterns and moisture convergence, resulting in a constrained northward migration of the ITCZ during the boreal summer, suppressing large scale rainfall patterns over many northern hemispheric monsoon regions and (as a related consequence) promoting increased rainfall in the above-described band from the equator southward (Liu et al., 2016; Oman et al., 2006; Graf, 1992; Dogar, 2018). This is consistent with analyses of Colose et al. (2016), who demonstrated that a hemispherically asymmetric volcanic forcing creates energetically deficient conditions in the hemisphere of the greatest forcing and which “pushes” the ITCZ away from it. It has also been shown with palaeoclimatic data that tropical and northern hemisphere eruptions can create a dipole that results in wetter summer conditions over extensive parts of the Mediterranean, with correspondingly drier conditions over northern Europe (Rao et al., 2017). This is also largely consistent with our model output (fig 9).

3.6 African monsoon and Nile River response

Our modeling suggests that all four eruptions during the period 168-158 BCE are likely to have strongly influenced the rainfall pattern over different monsoon rainfall regions in the northern hemisphere consecutively for 2-3 years after each eruption, and in combination produced a sustained deficit in monsoon rainfall (on average) for more than a decade. We now focus on the North African monsoon region, which strongly affects the Nile River summer flooding. Fig 10 shows the 3 consecutive years of monsoon season (JJAS) rainfall over equatorial and northern Africa (encompassing the Nile River basin) after each eruption. The African monsoon exhibited a strong response with reduced rainfall of more than 1 mm/day following the (mid-June) E1 tropical eruption in the year of the eruption itself (Year 0, fig 10), affecting both the White Nile watershed in the south of the basin and the Blue Nile and Atbara River watersheds further north and east in the Ethiopian Highlands. Reduced precipitation was also observed following each of the (also mid-June) extratropical eruptions (E2-E4) during the eruption years but was more spatially constrained (and particularly for E2, less severe). This result is perhaps unsurprising as the estimated SO_2 output of E2-E4 is only approximately 1/3 that of the tropical eruption, E1. Nonetheless in each case the Blue Nile and Atbara River headwaters in the Ethiopian highlands were observed to

Deleted: observations by

Deleted: regional

Deleted: shows

Deleted: to

Deleted: is

Deleted: ,

Deleted: is

Deleted: are

experience a statistically significant decrease, with important implications for the summer flood in Egypt, which depends for approximately 80% of its floodwater on rainfall here (Melesse et al., 2011). For E2-E4, this response was seen to intensify in the first post-eruption year, persisting into the second post-eruption year, while for E1 the response contracted geographically to resemble the response seen after E2-E4 (fig 9, fig 10). These results are indicative of an effective suppression of the African monsoon following tropical and northern hemispheric extratropical volcanic eruptions, a finding consistent with previous studies (e.g., Colose et al., 2016; Oman et al., 2006; Haywood et al., 2013; Jacobson et al. 2020; Manning et al., 2017).

Deleted: flooding

Deleted: can be

Deleted: contracts

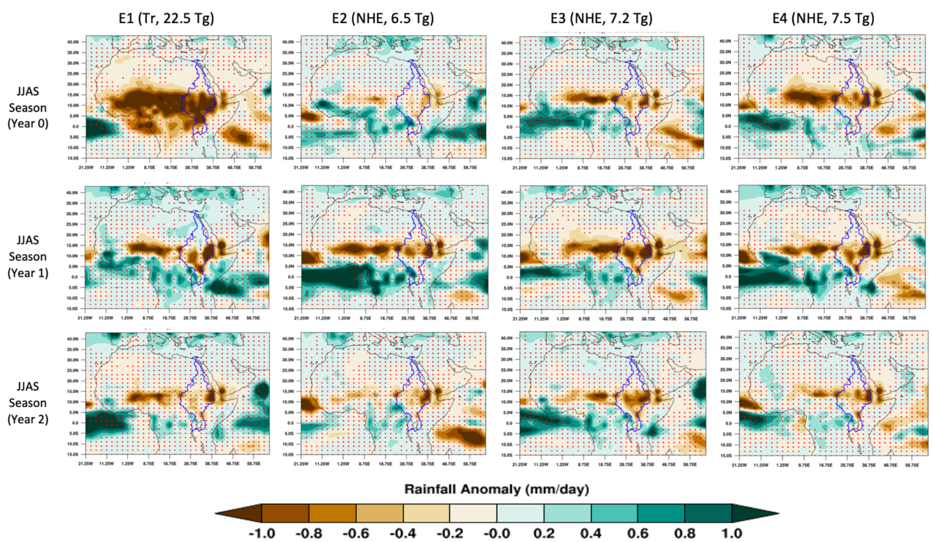

Fig 10. Ensemble mean rainfall difference from the climatological control for each of the first three monsoon seasons (JJAS; rows) after each eruption (columns) over equatorial and North Africa. The blue boundary line shows the present-day Nile River basin, which is broadly similar to the river extent approximately 2.5ka years ago. The red stippling indicates the regions over which change in rainfall is not significant at a 95% confidence level.

Spatial patterns of total cloud cover (Fig S7) for the three consecutive post-eruption monsoon seasons show a cloud cover decrease of up to 10% over East Africa and the adjacent Indian Ocean region. These spatial patterns are consistent with the above-reported negative rainfall anomalies (>1 mm/day) over North African land regions, especially over the watershed of the Nile River basin, and again suggest a strong weakening of the summer monsoon (Graf, 1992, Oman et al., 2005). Positive anomalies of total cloud cover also coincide with regions observed as having a positive rainfall response (e.g., Mediterranean and Middle East).

We also analyzed the mass of total water flow averaged over the Nile River basin (blue line, fig 11) as being representative of Nile flooding and river discharge at the river's mouth at an annual scale to summarize the volcanic impacts on Nile flooding. Table 2 thus presents the percentage deficit (-) or excess (+) of water flow in the Nile River basin on an annual basis after each eruption along with the variability (one standard deviation) observed across the model ensemble members, relative to the 100 years climatological mean (base climate). The tropical eruption (E1) had a strong impact (>30% deficit) on the annual water mass over the Nile catchment during the eruption year and first full post-eruption year (i.e., Years 0 and 1, table 2), with a more moderate decrease of ~13% during the second full post-eruption year (i.e., Year 2, table 2). The first extratropical eruption (E1) showed a minor decrease in the eruption year (Year 0, table 2) but this was not deemed statistically significant. The following two full post-eruption years reversed this pattern to exhibit a modest increase, but this was also not deemed statistically significant. The next two extratropical eruptions (E3 and E4) instead showed a more consistent response in the form of a decrease. For E3 and E4 this decrease was on the order of ~-5% in the eruption year (i.e., Year 0, table 2) and was notably greater in the first full post-eruption year (i.e., Year 1, table 2) for both E3 and E4 (being ~ -18% and ~ -12%, respectively). The decrease persisted into the second full post-eruption year (i.e., Year 2, table 2) for E4 (~-12%) but effectively fell back in line with the 100 years climatological mean for E3 (although this annual whole-basin mean change does exhibit the highest observed variance among ensemble members (table 2)). Several individual ensemble members have simulated the change in river flow at the 95% confidence levels (1.95*σ_{ctrl}; σ denotes standard deviation) for a few years when compared against the variability for the control period.

Deleted: Indian

Deleted: has

Deleted: to

Deleted: shows

Deleted: is

Deleted: reverse

Deleted: which is

Deleted: show

Deleted: is

Deleted: is

Deleted: ~-

Deleted: ~-

Deleted: persists

Deleted: falls

Table 2. Annual mean change (%) and standard deviation in water mass flow over the Nile River catchment for 3 consecutive years after each eruption. Control run variability (interannual standard deviation about the decadal mean, σ_{ctrl}) for Nile basin river flow is 25.2%.

	E1(Tr, 22.5 Tg) Change /Std	E2(NHE, 6.5 Tg) Change /Std	E3(NHE, 7.2 Tg) Change /Std	E4(NHE, 7.5 Tg) Change /Std
Year 0 (eruption year, mid-June)	-28.7±39.9	-3.02±22.5	-4.9±35.2	-4.7±29.6
Year 1	-37.8±22.5	2.5±36.7	-18.1±28.9	-11.7±29.9
Year 2	-13.4±32.2	10.7±39.9	0.9±47.8	-12.1±28.0

The spatial patterning of response across a basin as complex as the Nile is a critical further consideration (Fig 11). After the tropical eruption (E1), the above-described rainfall suppression can be associated with a drastic reduction in annual river flow observed over effectively the entire river basin, with a simulated decrease of approximately 30, 40 and 15 km^3 per year relative to the 100 years climatological mean (~104 km^3) for Years 0 to 2, respectively. After the second eruption (E2), the total annual river flow in Year 0 was observed to slightly increase (table 2), although this response was not statistically significant, and in Year 1 exhibited a marked contrast between (particularly) the southern (greater flow) and northern (lesser flow) parts of the basin, before a more consistent increased flow was observed in Year 2. The contrast between a reduced flow over (broadly) the northern part of the basin versus increased flow over the southern part was then observed consistently for all post eruption years shown in fig 11 for both eruptions E3 and E4. We can hypothesize that this contrast arises in large part as a function of the size and complexity of the Nile basin (and the markedly different geographical location of rainfall supplying the White Nile to the south and Blue Nile and Atbara River to the northeast), combined with the asymmetrical loading of sulfate aerosols in the higher latitudes of the northern hemisphere after extratropical eruptions. This may lead to a post-eruption scenario in which the northward boreal summer migration of the ITCZ and associated rain-bearing monsoon winds were suppressed (as discussed earlier). Given that these winds are the primary driver of summer rainfall over the Ethiopian highlands, the summer flooding of the Blue

Deleted: fig
Deleted: previously
Deleted: is
Deleted: decrease
Deleted: is
Deleted: is
Deleted: exhibits
Deleted: is
Deleted: is
Deleted: are

Nile and Atbara River into the north of the basin and Egypt would be diminished, while water flow down the White Nile (fed by rainfall over the equatorial lakes) would be potentially enhanced by the failure of the ITCZ to migrate northward beyond this region.

Deleted: will
Deleted: will

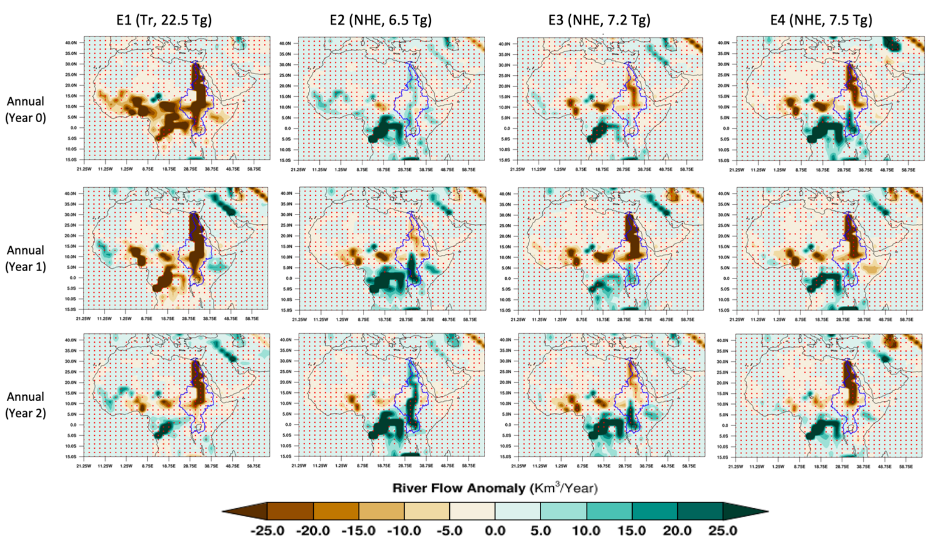

Fig 11. Annual river flow anomaly (km^3/year) relative to the control climatology for 3 consecutive years after each eruption (columns) over the North African continent. Other details are same as Fig 10.

Deleted: from

To summarize, the hydroclimatic impact of these four sequential volcanic eruptions on the Nile River basin, Fig 12 (top panel) shows that the northern hemisphere experienced a substantial cooling of ~2.5° C (1.0° C greater than the global average response) with a lower spread among ensembles after the first eruption (E1). The subsequent eruptions (E2, E3, and E4), reoccurring at equal temporal intervals, then maintained a cooling of ~1.75°C for at least a decade. The monthly anomaly of mean rainfall over the Nile basin was observed as a considerable decrease varying between ~1.0 and 1.5 mm/day during the monsoon seasons (JJAS) for the years following each eruption (Figure 12, middle panel). The impact of decreased rainfall over this region is strongly evident after the tropical eruption E1 in terms of Nile River

Deleted: the story of
Deleted: occurring
Deleted: is
Deleted: of
Deleted: to
Deleted: season

discharge at the river mouth (grid box centered at 29.0N, 31.25E) in the Nile delta region of Egypt (Fig 12, bottom panel). Our modelling shows here a mean deficit that begins in the year of the eruption (i.e., Year 0) and peaks at a reduction of more than 50% of water discharge during the first full post-eruption year (i.e., Year 1) effectively requiring 2 further years to recover. There is no persistent negative discharge anomaly evident after the second eruption (E2), although individual ensemble variability around the mean is quite high here. By contrast, a deficit is observed to begin in the year of the third eruption (E3, i.e., Year 0) that then persists throughout the first full post-eruption year (i.e., Year 1) and into the start of the second full post-eruption year (i.e., Year 2). This deficit peaks in Year 2 at just less than 50%. A similar response is observed after the fourth (E4) eruption, with a persistent negative anomaly starting in the first full post-eruption year (i.e., Year 1), continuing throughout Year 2 and into the start of Year 3. This deficit also peaks in Year 1 (at approximately 30%).

Deleted: that takes

Deleted: .

Deleted: %.

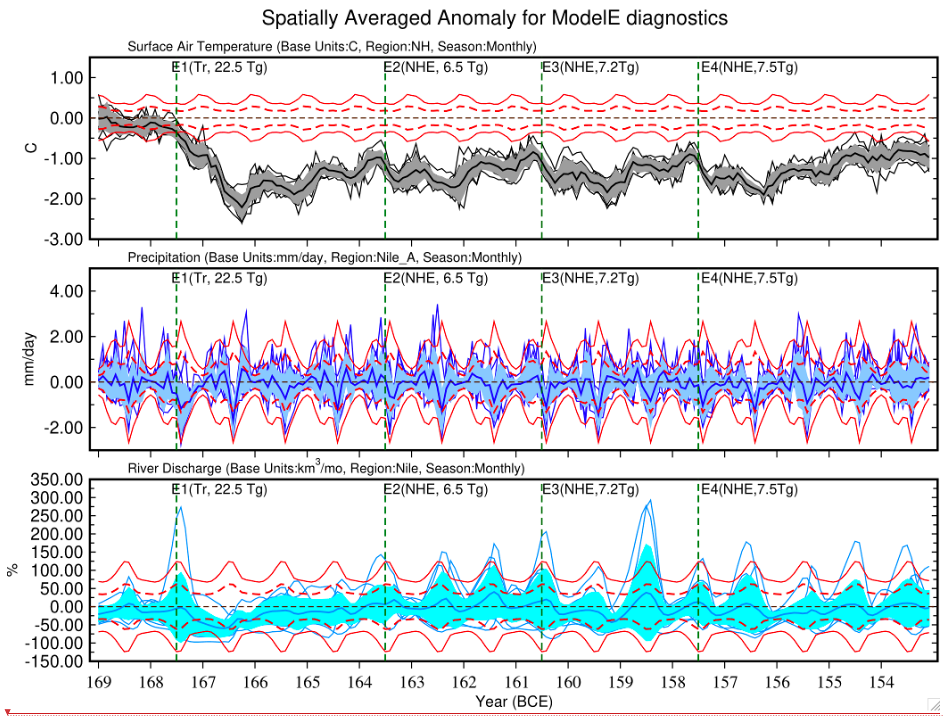

Fig 12: Monthly time series of individual ensemble and mean of surface temperature response (˚C) averaged over northern hemisphere (NH) (top panel), rainfall change (mm/day) for the model's spatial box representing the Nile River watershed (Latitude: (5N, 18N), Longitude: (30E, 42E)) (middle panel) and Nile River discharge anomaly (%) at the delta region (grid box centered at 29.0N, 31.25E). For each panel, the darker solid (thick) line shows the multi-ensemble mean, individual member (thin line), and the color envelope shows the associated variability (±σ; Standard deviation). The annual cycle of climate variability of the control run is shown as $1\sigma_{ctrl}$ (red dashed line) and $2\sigma_{ctrl}$ lines (red solid line) along the x-axis for all three variables. The vertical dotted green line shows when each eruption happened.

It is evident that the mean surface temperature response in the northern hemisphere is significant at the control period's $1\sigma_{ctrl}$ and $2\sigma_{ctrl}$ levels. However, while rainfall and river discharge responses are

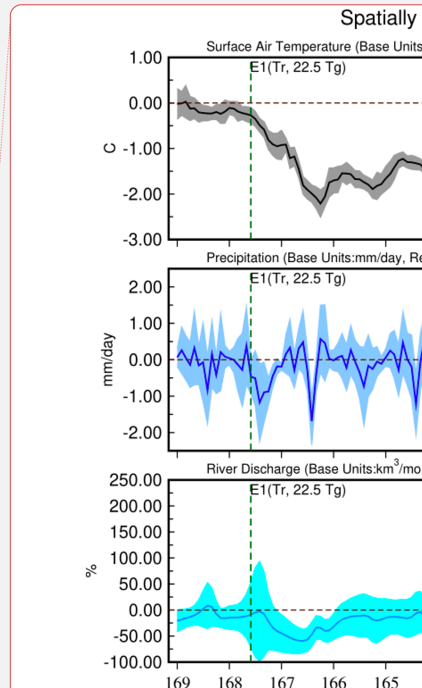

Deleted:

Deleted: mean

Deleted: over

Deleted: over

Deleted: The dark

Deleted: ((±σ;

Deleted: happens

Deleted:

significant at the $1\sigma_{ctrl}$ level, they fall within the $2\sigma_{ctrl}$ levels, although a few individual members do show significance at $2\sigma_{ctrl}$ as well. However, the statistical significance of the rainfall and discharge response may be sensitive to the dearth in the modeling Nile River basin at a relatively coarse resolution of the GISS ModelE, as well as the boundaries chosen to model the Nile basin and its headwaters. In particular, given the complexity of the Nile's hydrology and disparate sources of discharge for the White and Blue Niles. We thus investigated the post-volcanic change in river flow for the southern (White Nile-dominated) and northern (Blue Nile and Atbara river-dominated) parts of the basin by dividing it at 10° N (Fig 13). Annual mean river flow change for the south (blue lines) and north (red lines) of the Nile basin were in broad agreement with a negative flow anomaly after eruption E1. This was most notable in the eruption year and the first year following, with the 95th percentile envelopes (dotted lines) deemed significant at the 95% confidence level for both these years (i.e., crossing the dashed lines parallel to the x-axis (Fig 13). In contrast, the mean north and south responses disagreed, including in the sign of the observed changes, after the extratropical eruptions (E2, E3 & E4). More specifically, while the mean flow anomalies in the year of E2 were unremarkable and showed little north-south contrast, a more notable divergence was observed in the first year following, with a positive flow anomaly in the south and negative in the north. In the year of E3, flow in the south showed no notable anomaly, while flow in the north was marginally negative. This distinction became more marked in the first year following, mainly due to a larger negative anomaly in the north. In the year of E4, a negative anomaly was again observed in the north, persisting for three post-eruption years, and contrasting with positive or unremarkable anomalies in the south.

These results are consistent with our earlier-described results (e.g., spatial rainfall variability over the Nile River basin, as per Figs. 10 and 11) and proposed mechanisms, alongside expectations from the literature (e.g., Manning et al., 2017). Thus, tropical eruptions (like E1) may result in a more consistent (negative) north-south flow response due to their more even interhemispheric aerosol burden and associated radiative impact. Extratropical NH eruptions (like E2-E4) that can result in a more asymmetric hemispheric aerosol burden may, by contrast, introduce contrasting flow anomalies by suppressing the northward migration of the ITCZ, negatively impacting flow in the Blue Nile and Atbara rivers by diminishing monsoon rainfall in the Ethiopian highlands, while potentially enhancing flow in the White Nile, fed by rainfall over the equatorial lakes.

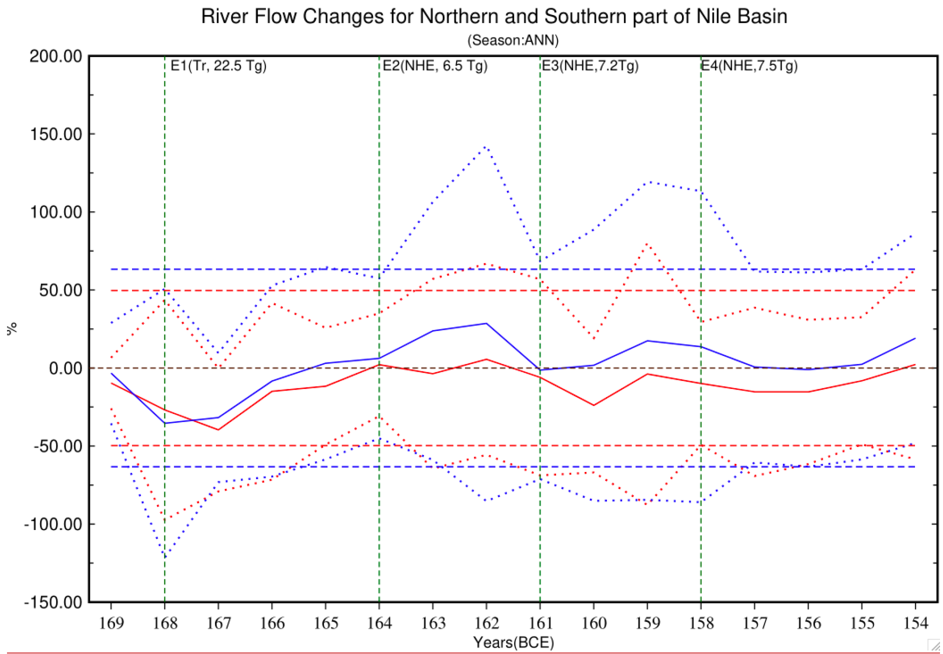

Fig 13. Annual Nile River flow changes averaged over the northern (red) and southern (blue) parts of the basin (divided at 10° N) for the entire simulation period. The solid lines represent the ensemble mean for each part of the basin; the dotted lines are ±1.95σ, where σ is derived from across all the ensembles, and the horizontal dashed lines parallel to x-axis are the ±1.95σ_{ctrl} where σ_{ctrl} is the standard deviation across the 100-year control run. Red and blue lines correspond to the northern and southern parts of the Nile basin, respectively.

4. Discussion and Conclusions

Recent years have seen increasing interest in the role of hydroclimatic variability in human history, including by interdisciplinary teams combining evidence and methods from across traditional disciplinary divides (e.g., McCormick, 2011, 2019; Manning et al., 2017; Ludlow and Travis, 2019; van Bavel et al., 2019; Degroot et al., 2021; Ljungqvist et al., 2021; Izdebski et al., 2022, Travis et al., 2022). For the pre-modern era, when systematic observations of hydroclimate become scarce, this effort depends increasingly upon natural archives (palaeoclimatic proxies) that track variability at spatial and temporal resolutions sufficiently high, and boasting sufficiently accurate dating, to convincingly identify associations with societal phenomena (e.g., subsistence crises, migration, conflict), economic and demographic processes, and major historical events (e.g., the "collapse" of kingdoms and empires). Work such as that by PAGES2k Network members offering paleoclimatic reconstructions and curated data collections (e.g., PAGES 2k Consortium, 2013; PAGES 2k Consortium, 2017) are thus crucial, although here the exclusive focus on the past 2k years (for some proxies an artificial horizon and for others an aspiration as temporal coverage and sampling depth improves), presently excludes some of the most foundational periods and events in human history. This includes the development of advanced ancient societies in Asia, the Near East and Mediterranean that are richly documented and hence offer considerable potential for the study of socioecological systems.

Important work has still been possible using speleothems, sedimentary and other archives (e.g., Drake, 2012; Schneider and Adali, 2014; Knapp and Manning, 2016; Sołtysiak, 2016), but there is often little direct temporal and/or geographical overlap between these early ancient world regions of rich human documentation and proxies (e.g., tree-ring based) with precision and accuracy at annual-or-better resolutions. A major recent advance, however, has been the publication of a chronologically precise and accurate bipolar ice-core-based volcanic forcing reconstruction for the past 2,500 years (Sigl et al., 2015; Toohey and Sigl, 2017). The potentially global hydroclimatic impacts of major explosive eruptions makes this record widely geographically relevant, while the repeated incidence of major eruptions that can now be seen in ever greater detail through sulphate deposition in the polar ice sheets has allowed their use as "tests" of societal vulnerability and response to sudden hydroclimatic shocks in both a statistical manner (e.g., Manning et al., 2017; Gao et al., 2021; Ludlow et al., in-press, 2022) and in a complementary qualitative manner as "revelatory crises" (Solway, 1994; Dove, 2014), in which tensions, inequalities and vulnerabilities in given political and economic systems are potentially exposed under the pressure of sudden environmental variability (e.g., Ludlow and Crampsie, 2019; Ludlow et al., in-press, 2022;

Huhtamaa et al., 2022). The scrutiny that such exposure can bring to prevailing human systems (social, economic, ideological) can spur their potentially rapid transformation, while the related suspension of cultural norms and business-as-usual practices under the “state of exception” that may prevail during “natural” disasters and other crises can facilitate this, though such conditions can also be exploited to further entrench existing power bases (e.g., Dove, 2014; McConnell et al., 2020).

For historical eruptions to act as tests or be studied as potential “revelatory” crises, knowledge of their dating alone is insufficient, particularly given the regional and seasonal variability of volcanic hydroclimatic impacts, and the sensitivity of these impacts to multiple variables such as the location, season, chemical composition, and height attained by volcanic ejecta (Robock, 2000; Cole-Dai, 2010; Ludlow et al., 2013). Even where instrumental or natural archives are available, but especially where these are thin or absent, climate modelling can provide insights into the expected climatic impacts for particular regions, seasons and related physical (e.g., riverine) systems. This is true for modelling of idealized eruptions, but potentially even more so for models that produce “historical realizations” based upon actual forcing reconstructions (e.g., Tardif et al., 2019).

In this context we have presented a modeling effort that explores the impacts of a unique eruption quartet during the (historically tumultuous) decade 168-158 BCE, with a particular focus on the Nile River basin. These target years are intermediate between the mid-Holocene and end of the preindustrial periods, and representative background climate conditions are necessary to investigate the climatic impact of such a short-term forcing (Zanchettin et al., 2013). PMIP4 vegetation distributions (linearly interpolated for the 2.5ka period from the mid-Holocene (Otto-Bliesner et al., 2017) to the end of the preindustrial (taken as 1850) for the GISS ModelE2.1 (MATRIX) version (Kelley et al., 2020; Bauer et al., 2020) were therefore used to improve GCM simulations without a fully dynamic vegetation implementation (Harrison et al., 2015). Vegetation-albedo feedbacks due to a greater prevalence of arid shrubs/steppe over Africa and of boreal forests over high latitudes were thus observed to induce a northward movement of the ITCZ over Africa (Sahara region) promoting a simulated rainfall increase of the order of 0.5-1.0 mm/day in the region (such a response is consistent with theoretical expectations and other estimates (e.g., Otterman 1975; Charney 1975; Claussen 2009; Pausata et al., 2016; Rachmayini et al., 2015).

Deleted:)).

The GISS ModelE2.1 simulated a strong shortwave and longwave global radiative forcing of -10 and +3.0 W/m^2, respectively, following the tropical eruption (E1) and a roughly equal forcing of -3.5 and +1.0 W/m^2, respectively, for each of the 3 extratropical eruptions (E2-E4). The peak net radiative volcanic forcing was calculated at -7.5 W/m^2 and -2.5 W/m^2 for the tropical and extratropical eruptions, respectively. The model calculated a global AOD at 550 nm of 0.22 and 0.1 after the tropical and extratropical eruptions, respectively, and estimated a peak cooling of ~1.5 ºC almost 12-months after the first eruption (E1), with the three consecutive eruptions then sustaining a surface cooling of about 1.0 ºC for almost all of the 15 years of simulations. The first eruption (E1) was 30% larger than Pinatubo and the GISS ModelE2.1 simulated proportionally stronger radiative impacts as compared to Pinatubo (for details of which, see: Hansen et al., 1992; Robock and Mao 1994; Parker et al., 1996; McCormick et al., 1995; Stenchikov, 2015). A detailed analysis of the impacts of volcanic aerosols on the chemical composition of the stratosphere was not part of this study.

The global hydrological cycle responds vigorously to the volcanically induced surface cooling in the GISS ModelE2.1, with a greater than 1.0 mm/day decrease observed in rainfall over the African, Indian, and Chinese regions during the summer monsoon season consecutively for 3 years after eruption E1 (tropical) and for 2 years after each of the eruptions E2-E4 (extratropical northern hemispheric). Statistically significant decreases in rainfall over the major tropical northern hemisphere rain belt was also calculated by the model, as well as more broadly over higher latitudes for this hemisphere. Some smaller regions of positive rainfall anomalies were, however, simulated over the northern hemisphere mid-latitudes (both land and ocean) around 30º N. These patterns of hydrological cycle response are consistent with previous studies reporting changes in rainfall and large-scale atmospheric circulations (such as Hadley cell weakening) (e.g., Robock and Liu, 1994; Gillett et al., 2004; Trenberth and Dai, 2007; Crowley et al., 2008; Fischer et al., 2008; Joseph and Zeng, 2011; Timmreck, 2012; Iles et al., 2012, Haywood et al., 2013; Liu et al., 2016).

For the equatorial and northern African landmass specifically, the GISS ModelE2.1 produced a notable suppression of monsoon (JJAS) rainfall for all eruptions, E1-E4. The onset of this response can be observed in the JJAS season beginning with each eruption year itself, though the timing of the peak intensity and/or greatest spatial extent of this suppression varied between eruptions (e.g., for E1 the

Deleted: parker

Deleted: -

Deleted: is

Deleted: are

Deleted: produces

Deleted: can vary

greatest extent and peak intensity occurred for JJAS in Year 0, while for E2-E3 the peak intensity and greatest extent occurred in Year 1, and for E4 in Year 0). The suppression centered (for all eruptions and each plotted post-eruption JJAS season, fig 10) around latitudes 10-15°N, where it ran in an east-west band that in some years was effectively contiguous across the continent (approx. 16°W to 52°E). There was, however, a tendency for this response to be more marked and long-lived (into JJAS of Year 2, fig 10) in the central and eastern portions of this range, where it is statistically significant and can surpass 1 mm/day (up to 30-40% of climatology for control period).

Importantly, the regions of the most rapid onset, greatest persistence and intensity of response included Lake Tana (12°0′N 37°15′E) and the Ethiopian highlands that comprise the headwaters of the Blue Nile and Atbara rivers and which supply the vast majority of summer floodwater in Egypt (Melesse et al., 2011). This result is broadly consistent with CMIP5 model runs forced with large twentieth century eruptions (e.g., Iles and Hegerl, 2014; Manning et al., 2017). Annual river flow for the Nile River basin (fig 11) closely followed the apparent patterns of decreased JJAS rainfall over the headwater region. Simulated river flow showed a deficit in the range of 15-40 km^3/year up to 3 years following the modelled extratropical northern hemisphere eruptions. Simulated variability in river discharge was also seen to increase 3/4-fold following the extratropical eruptions, because of the spatial variability in the rainfall response across ensemble members. There is no way to tell which ensemble member describes best the historical conditions that actually happened following the eruptions between 168 and 158 BCE, but the large variability and the statistical significance of the drying tells us that Nile summer flooding may have been considerably lower than the simulated mean anomaly.

What is nonetheless certain is that the scale and persistence of the hydroclimatic impacts implied by our modelling for the 168-158 BCE eruption quartet supports, to begin, inferences of poor Nile flooding in 166 and 161 BCE from scattered references in surviving written sources (Bonneau, 1971). These also identify 169 BCE as potentially experiencing poor flooding, which suggests (assuming sufficiently accurate ice-core dating (Sigl et al., 2015)) that the eruption quartet may have compounded any societal impacts already arising from this. Indeed, our modelling supports the contention that there is a largely overlooked but significant environmental context to what has long been recognized as a tumultuous decade in Egyptian history. Acknowledging the historical context evolving over the preceding decades,

Deleted: occurs

Deleted: occurs

Deleted: centers

Deleted: runs

Deleted: is

Deleted: is

Deleted: include

Deleted: follows

Deleted: shows

Deleted: is

and the resulting political, military, economic and cultural setting through which any hydroclimatic shock will have propagated, is of course also key to achieving a fuller understanding of the human-environmental entanglements in the 160s, as indeed it is for any period or region (White and Pei, 2020). This now more clearly includes the role of explosive volcanism and (relatedly) where along the spectrum of proximate to ultimate causality (as per Gao et al., 2021) any resulting hydroclimatic shocks lay in contributing to the revolts and other societal stressors in evidence. Thus, the increasing dominance of Rome in the eastern Mediterranean, and the growing internal political weakness of the Ptolemaic kingdom and their great rivals the Seleukid empire are writ large in the historical narrative of the second century BCE Mediterranean world, but the extent to which the instability of the major eastern Mediterranean powers was an outcome of the rising power of Rome has been heavily debated. A consensus view is now that these developments were directly coupled, and that eastward Roman expansion was driven not by the exceptional aggressiveness of Rome so much as by a "power transition crisis" in the eastern states around 207-200 BCE that drew Rome in (Eckstein, 2008).

Deleted: and thereafter, including the role of explosive volcanism.

The Ptolemies also began to face notable internal dynastic disputes and broader internal unrest among (at least certain sections of) the populace in the years after the Battle of Raphia in 217 BCE. Despite their success in that battle against the Seleukids at the close of the so-called Fourth Syrian War (Grainger, 2010), this was marked as a turning point for longer-term Ptolemaic fortunes by the Greek historian Polybius (V.107.1-3). The high cost of this war and subsequent continued conflict with the Seleukids (that also ultimately saw the Ptolemies lose control of important rain-fed agricultural regions such as Coele Syria that had given the kingdom some resilience to years of poor Nile flood), were important developments that likely increased their vulnerability to volcanic hydroclimatic shocks. Indeed, other eruptions such as a tropical eruption in 209 BCE (Sigl et al., 2015) occur conspicuously close to other major events such as the Great Theban Revolt that started ca.207 BCE (Manning et al., 2017), in which the Ptolemies lost control of Upper (i.e., southern) Egypt to two presumably native Egyptian kings until 187 BCE, with unrest also extending at times into the Delta region of Lower (i.e., northern) Egypt. During the 6th Syrian War, Antiochus IV and his Seleukid army invaded Egypt twice. The first invasion occurred in 170 BCE and the second, more serious occupation, occurred in 168 BCE. This takeover would have re-shaped Mediterranean history had it not been averted by Roman diplomatic intervention commonly referred to as "the Day of Eleusis" (Hölbl, 2001, pp.147-8).

It is against the background of these longer-term developments, to which explosive volcanism and hydroclimatic shocks also likely contributed (Ludlow and Manning, 2016; Manning et al., 2017; Ludlow and Manning, 2021), that our modelling allows us to more readily understand the internal turmoil in Egypt in the 160s and 150s BCE, affecting both the capital Alexandria and the countryside. Surviving sources refer, for example, to “bad times and been driven to every extremity owing to the price of wheat” in 168 BCE (*UPZ* 1 59; Bagnall and Derow, 2004, pp. 281-82), and it is known that by the middle of the decade an Egypt-wide agricultural crisis, described as a "calamity" was underway that drove Ptolemaic officials to near panic (*UPZ* 1 110, 165-164) BCE. Manning et al. (2017) have already identified dates of probable revolt onset in Ptolemaic history, with such onset dates identified in 168 BCE and 156 BCE both also coinciding closely with the dates of our eruption quartet. A study of the longevity and geography of these revolts is now of considerable interest. The surviving texts do not yet tell a complete story but scattered written references that suggest a long persistence of revolt throughout the decade, including for the years 168-157 BCE (Veïsse 2004, pp. 78-79), are now rendered more credible and explicable given the modelled persistence of reduced temperatures and suppressed Nile summer flooding for more than a decade following the 168 BCE tropical eruption and the three following extratropical NH eruptions.

Code/Data availability

Details to support the results in the manuscript is available as supplementary information is provided with the manuscript. Raw data and codes are available on request to author.

Acknowledgements

RS, KT, FL and JM acknowledge support by the National Science Foundation under Grant No. ICER-1824770. ANL acknowledges institutional support from NASA GISS. Resources supporting this work were provided by the NASA High-End Computing (HEC) Program through the NASA Center for Climate Simulation (NCCS) at Goddard Space Flight Center. The authors thank for their input through multiple discussions the project members and collaborators of the ICER-1824770 project, ‘Volcanism, Hydrology and Social Conflict: Lessons from Hellenistic and Roman-Era Egypt and Mesopotamia’. FL acknowledges support from the Trinity Center for Environmental Humanities. This paper benefited from discussion facilitated by the ‘Volcanic Impacts on Climate and Society’ (VICS) Working Group of PAGES.

Author’s contributions

FL and JM identified the study period in consultation with the other authors. RS, KT and ANL designed the model simulations. RS performed the simulations, created the figures in close collaboration with KT, ANL, FL and JM. RS wrote the first draft of the manuscript and led the writing of subsequent drafts. All authors contributed to the interpretation of results and the drafting of the text.

Competing interests

The authors declare no competing interests.

Short Summary

This study is a modelling effort to investigate hydroclimate impacts for the Nile River basin induced by a volcanic “quartet” of four closely spaced eruptions in ice-core volcanic chronology for the decade 168-158 BCE in a context to ancient Egyptian history. The NASA GISS ModelE simulated a strong response in sustained temperature reduction and suppressed monsoon rainfall over East Africa following these eruptions, leading to a deficit in Egypt's agriculturally critical Nile summer flooding.

References

Aquila, V., Oman, L. D., Stolarski, R. S., Colarco, P. R., and Newman, P. A.: Dispersion of the volcanic sulfate cloud from a Mount Pinatubo–like eruption, 117, https://doi.org/10.1029/2011JD016968, 2012.

Aquila, V., Oman, L. D., Stolarski, R., Douglass, A. R., and Newman, P. A.: The Response of Ozone and Nitrogen Dioxide to the Eruption of Mt. Pinatubo at Southern and Northern Midlatitudes, 70, 894–900, https://doi.org/10.1175/JAS-D-12-0143.1, 2013.

Bauer, S. E., Wright, D. L., Koch, D., Lewis, E. R., and McGraw, R.: MATRIX (Multiconfiguration Aerosol TRacker of mIXing state): an aerosol microphysical module for global atmospheric models, 33, 2008.

Bauer, S. E., Ault, A., and Prather, K. A.: Evaluation of aerosol mixing state classes in the GISS modelE-MATRIX climate model using single-particle mass spectrometry measurements, 118, 9834–9844, https://doi.org/10.1002/jgrd.50700, 2013.

Bauer, S. E., Tsigaridis, K., Faluvegi, G., Kelley, M., Lo, K. K., Miller, R. L., Nazarenko, L., Schmidt, G. A., and Wu, J.: Historical (1850–2014) Aerosol Evolution and Role on Climate Forcing Using the GISS ModelE2.1 Contribution to CMIP6, 12, e2019MS001978, https://doi.org/10.1029/2019MS001978, 2020.

Bell, B. 1975. 'Climate and the History of Egypt: The Middle Kingdom', *American Journal of Archaeology* 79(3): 223-69.

Berhane, F., Zaitchik, B., and Dezfuli, A.: Subseasonal Analysis of Precipitation Variability in the Blue Nile River Basin, 27, 325–344, https://doi.org/10.1175/JCLI-D-13-00094.1, 2014.

Blouin, J.: Defining and measuring tax planning aggressiveness, 67, 875–899, https://doi.org/10.17310/ntj.2014.4.06, 2014.

Bluth, G. J. S., Doiron, S. D., Schnetzler, C. C., Krueger, A. J., and Walter, L. S.: Global tracking of the SO2 clouds from the June, 1991 Mount Pinatubo eruptions, 19, 151–154, https://doi.org/10.1029/91GL02792, 1992.

Braconnot, P., Joussaume, S., Marti, O., and de Noblet, N.: Synergistic feedbacks from ocean and vegetation on the African Monsoon response to Mid-Holocene insolation, 26, 2481–2484, https://doi.org/10.1029/1999GL006047, 1999.

Brenna, H., Kutterolf, S., Mills, M. J., and Krüger, K.: The potential impacts of a sulfur- and halogen-rich supereruption such as Los Chocoyos on the atmosphere and climate, 20, 6521–6539, https://doi.org/10.5194/acp-20-6521-2020, 2020.

Broccoli, A. J., Dahl, K. A., and Stouffer, R. J.: Response of the ITCZ to Northern Hemisphere cooling, 33, https://doi.org/10.1029/2005GL024546, 2006.

Butzer, K. W.: Early hydraulic civilization in Egypt: a study in cultural ecology, The University of Chicago Press, Chicago London, 134 pp., 1976.

Butzer, K.W. 1984. 'Long-term Nile flood variation and political discontinuities in pharaonic Egypt', in: J. Desmond Clark and S.A. Brandt (eds.), *From Hunters to Farmers: The Causes and Consequences of Food Production in Africa*, Berkeley, 102-12.

Charney, J. G.: Dynamics of deserts and drought in the Sahel, 101, 193–202, https://doi.org/10.1002/qj.49710142802, 1975.

Christiansen, B.: Volcanic Eruptions, Large-Scale Modes in the Northern Hemisphere, and the El Niño–Southern Oscillation, 21, 910–922, https://doi.org/10.1175/2007JCLI1657.1, 2008.

Chiang, J. C. H. and Bitz, C. M.: Influence of high latitude ice cover on the marine Intertropical Convergence Zone, Climate Dynamics, 25, 477–496, https://doi.org/10.1007/s00382-005-0040-5, 2005.

Campbell, B. M. S. and Ludlow, F. (2020) "Climate, Disease and Society in Late-Medieval Ireland", Proceedings of the Royal Irish Academy, 120C, 159-252.

Claussen*, M.: Late Quaternary vegetation-climate feedbacks, 5, 203–216, https://doi.org/10.5194/cp-5-203-2009, 2009.

Claussen, M., Brovkin, V., Ganopolski, A., Kubatzki, C., and Petoukhov, V.: Climate Change in Northern Africa: The Past is Not the Future, Climatic Change, 57, 99–118, https://doi.org/10.1023/A:1022115604225, 2003.

Cole- Dai J., 'Volcanoes and Climate', WIREs Climate Change , 1, 824– 39, 2010.

Colose, C. M., LeGrande, A. N., and Vuille, M.: Hemispherically asymmetric volcanic forcing of tropical hydroclimate duringthe last millennium, Earth Syst. Dynam., 7, 681–696, https://doi.org/10.5194/esd-7-681-2016, 2016.

Crowley, T., GA, Z., Vinther, B., Udisti, R., Kreutzs, K., Cole-Dai, J., and Castellano, E.: Volcanism and the Little Ice Age, PAGES Newslett., 16, 22–23, https://doi.org/10.1029/2002GL0166335, 2008.

D'Arrigo, R., Seager, R., Smerdon, J. E., LeGrande, A. N., and Cook, E. R.: The anomalous winter of 1783–1784: Was the Laki eruption or an analog of the 2009–2010 winter to blame?, 38, https://doi.org/10.1029/2011GL046696, 2011.

Dogar, M. M.: Impact of Tropical Volcanic Eruptions on Hadley Circulation Using a High-Resolution AGCM, 114, 1284, https://doi.org/10.18520/cs/v114/i06/1284-1294, 2018.

Dove M. R.: *Anthropology of Climate Change* (Chichester, Wiley & Sons, 2014).

Degroot, D., Anchukaitis, K., Bauch, M., Burnham, J., Carnegy, F., Cui, J., de Luna, K., Guzowski, P., Hambrecht, G., Huhtamaa, H., Izdebski, A., Kleemann, K., Moesswilde, E., Neupane, N., Newfield, T., Pei, Q., Xoplaki, E., and Zappia, N.: Towards a rigorous understanding of societal responses to climate change. Nature, 591, 539–550, doi:10.1038/s41586-021-03190-2, 2021.

Drake, B.L: 'The Influence of Climatic Change on the Late Bronze Age Collapse and the Greek Dark Ages', *Journal of Archaeological Science* 39, pp.1862-1870, 2012

A. Eckstein, Rome enters the Greek East: From Anarchy to Hierarchy in the Hellenistic Mediterranean, 230-170 BC. Blackwell, 2008.

English, J. M., Toon, O. B., and Mills, M. J.: Microphysical simulations of large volcanic eruptions: Pinatubo and Toba, 118, 1880–1895, https://doi.org/10.1002/jgrd.50196, 2013.

Eyring, V., Bony, S., Meehl, G. A., Senior, C. A., Stevens, B., Stouffer, R. J., and Taylor, K. E.: Overview of the Coupled Model Intercomparison Project Phase 6 (CMIP6) experimental design and organization, Geosci. Model Dev., 9, 1937–1958, https://doi.org/10.5194/gmd-9-1937-2016, 2016.

Fischer, E. M., Luterbacher, J., Zorita, E., Tett, S. F. B., Casty, C., and Wanner, H.: European climate response to tropical volcanic eruptions over the last half millennium, 34, https://doi.org/10.1029/2006GL027992, 2007.

Fujiwara, M., Hibino, T., Mehta, S. K., Gray, L., Mitchell, D., and Anstey, J.: Global temperature response to the major volcanic eruptions in multiple reanalysis data sets, Atmos. Chem. Phys., 15, 13507–13518, https://doi.org/10.5194/acp-15-13507-2015, 2015.

Gao, F., Morisette, J. T., Wolfe, R. E., Ederer, G., Pedelty, J., Masuoka, E., Myneni, R., Tan, B., and Nightingale, J.: An Algorithm to Produce Temporally and Spatially Continuous MODIS-LAI Time Series, 5, 60–64, https://doi.org/10.1109/LGRS.2007.907971, 2008.

Gao, C., Ludlow, F., Matthews, A., Stine, A. R., Robock, A., Pan, Y., Breen, R. and Sigl. M. (2021) "Volcanic Climate Impacts Can Act as Ultimate and Proximate Causes of Chinese Dynastic Collapse", Communications Earth & Environment, 2, Article Number: 234. DOI: 10.1038/s43247-021-00284-7

Gillett, N. P., Weaver, A. J., Zwiers, F. W., and Wehner, M. F.: Detection of volcanic influence on global precipitation, 31, https://doi.org/10.1029/2004GL020044, 2004.

Guillet, S., Corona, C., Ludlow, F., Oppenheimer, C., and Stoffel, M.: Climatic and societal impacts of a “forgotten” cluster of volcanic eruptions in 1108-1110 CE, Sci Rep, 10, 6715, https://doi.org/10.1038/s41598-020-63339-3, 2020.

Guo, S., Bluth, G. J. S., Rose, W. I., Watson, I. M., and Prata, A. J.: Re-evaluation of SO2 release of the 15 June 1991 Pinatubo eruption using ultraviolet and infrared satellite sensors, 5, https://doi.org/10.1029/2003GC000654, 2004.

Gu, G. and Adler, R. F.: Precipitation and Temperature Variations on the Interannual Time Scale: Assessing the Impact of ENSO and Volcanic Eruptions, 24, 2258–2270, https://doi.org/10.1175/2010JCLI3727.1, 2011.

Graf, H.-F.: Arctic radiation deficit and climate variability, Climate Dynamics, 7, 19–28, https://doi.org/10.1007/BF00204818, 1992.

Graft, H.-F., Kirchner, I., Robock, A., and Schult, I.: Pinatubo eruption winter climate effects: model versus observations, Climate Dynamics, 9, 81–93, https://doi.org/10.1007/BF00210011, 1993.

Graf, H.-F., Li, Q., and Giorgetta, M. A.: Volcanic effects on climate: revisiting the mechanisms, 7, 4503–4511, https://doi.org/10.5194/acp-7-4503-2007, 2007.

Grainger, J. The Syrian Wars (Brill, 2010).

Hansen, J. E., Lacis, A. A., Lee, P., and Wang, W.-C.: Climatic Effects of Atmospheric Aerosols, 338, 575–587, https://doi.org/10.1111/j.1749-6632.1980.tb17151.x, 1980.

Hansen, J., Lacis, A., Ruedy, R., and Sato, M.: Potential climate impact of Mount Pinatubo eruption, 19, 215–218, https://doi.org/10.1029/91GL02788, 1992.

Hassan, F. A.: Nile Floods and Political Disorder in Early Egypt, in: Third Millennium BC Climate Change and Old World Collapse, Berlin, Heidelberg, 1–23, https://doi.org/10.1007/978-3-642-60616-8_1, 1997b.

Hassan, F.A. 1997a. ‘The Dynamics of a Riverine Civilization: A Geoarchaeological Perspective on the Nile Valley, Egypt’, *World Archaeology* 29(1): 51-74.

Deleted: 1997

Hassan, F. A.: Extreme Nile floods and famines in Medieval Egypt (AD 930–1500) and their climatic implications, Quaternary International, 173–174, 101–112, https://doi.org/10.1016/j.quaint.2007.06.001, 2007.

Harrison, S. P., Bartlein, P. J., Izumi, K., Li, G., Annan, J., Hargreaves, J., Braconnot, P., and Kageyama, M.: Evaluation of CMIP5 palaeo-simulations to improve climate projections, Nature Clim Change, 5, 735–743, https://doi.org/10.1038/nclimate2649, 2015.

Haywood, J. M., Jones, A., Bellouin, N., and Stephenson, D.: Asymmetric forcing from stratospheric aerosols impacts Sahelian rainfall, Nature Clim Change, 3, 660–665, https://doi.org/10.1038/nclimate1857, 2013.

Hewitt, C. D. and Mitchell, J. F. B.: A fully coupled GCM simulation of the climate of the mid-Holocene, 25, 361–364, https://doi.org/10.1029/97GL03721, 1998.

Hölbl, G. A History of the Ptolemaic Empire (Routledge, 2001).

Huhtamaa, H., Stoffel, M. and Corona, C. (2022). Recession or resilience? Long-range socioeconomic consequences of the 17th-century volcanic eruptions in northern Fennoscandia, *Climate of the Past Discussions*. https://doi.org/10.5194/cp-2021-147.

Iles, C. E., Hegerl, G. C., Schurer, A. P., and Zhang, X.: The effect of volcanic eruptions on global precipitation, 118, 8770–8786, https://doi.org/10.1002/jgrd.50678, 2013.

Iles, C. E. and Hegerl, G. C.: The global precipitation response to volcanic eruptions in the CMIP5 models, Environ. Res. Lett., 9, 104012, https://doi.org/10.1088/1748-9326/9/10/104012, 2014.

Ito, G., Romanou, A., Kiang, N. Y., Faluvegi, G., Aleinov, I., Ruedy, R., Russell, G., Lerner, P., Kelley, M., and Lo, K.: Global Carbon Cycle and Climate Feedbacks in the NASA GISS ModelE2.1, 12, e2019MS002030, https://doi.org/10.1029/2019MS002030, 2020.

Izdebski, A., Bloomfield, K., Eastwood, W. J., Fernandes, R., Fleitmann, D., Guzowski, P., Haldon, J., Ludlow, F., Luterbacher, J., Manning, J. G., Masi, A., Mordechai, L., Newfield, T., Stine, A. R., Senkul, C. and Xoplaki, E. (In Press, 2022), "The Emergence of Interdisciplinary Environmental History: Bridging the Gap between the Humanistic and Scientific Approaches to the Late Holocene," *Annales*, 77 (2), 1-48.

Jacobson, T. W. P., Yang, W., Vecchi, G. A., and Horowitz, L. W.: Impact of volcanic aerosol hemispheric symmetry on Sahel rainfall, Clim Dyn, 55, 1733–1758, https://doi.org/10.1007/s00382-020-05347-7, 2020.

Joseph, R. and Zeng, N.: Seasonally Modulated Tropical Drought Induced by Volcanic Aerosol, 24, 2045–2060, https://doi.org/10.1175/2009JCLI3170.1, 2011.

Jungclaus, J. H., Lorenz, S. J., Timmreck, C., Reick, C. H., Brovkin, V., Six, K., Segschneider, J., Giorgetta, M. A., Crowley, T. J., Pongratz, J., Krivova, N. A., Vieira, L. E., Solanki, S. K., Klocke, D., Botzet, M., Esch, M., Gayler, V., Haak, H., Raddatz, T. J., Roeckner, E., Schnur, R., Widmann, H., Claussen, M., Stevens, B., and Marotzke, J.: Climate and carbon-cycle variability over the last millennium, Clim. Past, 6, 723–737, https://doi.org/10.5194/cp-6-723-2010, 2010.

Kelley, M., Schmidt, G. A., Nazarenko, L. S., Bauer, S. E., Ruedy, R., Russell, G. L., Ackerman, A. S., Aleinov, I., Bauer, M., Bleck, R., Canuto, V., Cesana, G., Cheng, Y., Clune, T. L., Cook, B. I., Cruz, C. A., Genio, A. D. D., Elsaesser, G. S., Faluvegi, G., Kiang, N. Y., Kim, D., Lacis, A. A., Leboissetier, A., LeGrande, A. N., Lo, K. K., Marshall, J., Matthews, E. E., McDermid, S., Mezuman, K., Miller, R. L., Murray, L. T., Oinas, V., Orbe, C., García-Pando, C. P., Perlwitz, J. P., Puma, M. J., Rind, D., Romanou, A., Shindell, D. T., Sun, S., Tausnev, N., Tsigaridis, K., Tselioudis, G., Weng, E., Wu, J., and Yao, M.-S.: GISS-E2.1: Configurations and Climatology, 12, e2019MS002025, https://doi.org/10.1029/2019MS002025, 2020.

Kiang, N. Y.: Description of the NASA GISS vegetation dynamics model Tech. rep. NASA, 2012

Khodri, M., Izumo, T., Vialard, J., Janicot, S., Cassou, C., Lengaigne, M., Mignot, J., Gastineau, G., Guilyardi, E., Lebas, N., Robock, A., and McPhaden, M. J.: Tropical explosive volcanic eruptions can trigger El Niño by cooling tropical Africa, Nat Commun, 8, 778, https://doi.org/10.1038/s41467-017-00755-6, 2017.

Kilian, M., Brinkop, S., and Jöckel, P.: Impact of the eruption of Mt Pinatubo on the chemical composition of the stratosphere, 20, 11697–11715, https://doi.org/10.5194/acp-20-11697-2020, 2020.

Kim, Y., Moorcroft, P. R., Aleinov, I., Puma, M. J., and Kiang, N. Y.: Variability of phenology and fluxes of water and carbon with observed and simulated soil moisture in the Ent Terrestrial Biosphere Model (Ent TBM version 1.0.1.0.0), Biogeosciences, https://doi.org/10.5194/gmdd-8-5809-2015, 2015.

Kirtman, B., Power, S. B., Adedoyin, A. J., Boer, G. J., Bojariu, R., Camilloni, I., Doblas-Reyes, F., Fiore, A. M., Kimoto, M., Meehl, G., Prather, M., Sarr, A., Schar, C., Sutton, R., van Oldenborgh, G. J., Vecchi, G., and Wang, H.-J.: Chapter 11 - Near-term climate change: Projections and predictability, edited by: IPCC, Cambridge University Press, Cambridge, 2013.

Klock D: Assessing the uncertainty in climate sensitivity, Report on Earth System Science 95, Max Plank Institute of Meteorology ISSN 1614-1199, 87pp, Phd Thesis 2011.

Knapp, A.B.and Manning, S.W. :'Crisis in Context: The End of the Late Bronze Age in the Eastern Mediterranean', *American Journal of Archaeology* 120 pp.99-149, 2016.

Kostić, S., Stojković, M., Prohaska, S., and Vasović, N.: Modeling of river flow rate as a function of rainfall and temperature using response surface methodology based on historical time series, Journal of Hydroinformatics, 18, 651–665, https://doi.org/10.2166/hydro.2016.153, 2016.

Kutzbach, J., Bonan, G., Foley, J., and Harrison, S. P.: Vegetation and soil feedbacks on the response of the African monsoon to orbital forcing in the early to middle Holocene, Nature, 384, 623–626, https://doi.org/10.1038/384623a0, 1996.

Kutzbach, J. E. and Liu, Z.: Response of the African Monsoon to Orbital Forcing and Ocean Feedbacks in the Middle Holocene, 278, 440–443, https://doi.org/10.1126/science.278.5337.440, 1997.

Labitzke, K. and McCormick, M. P.: Stratospheric temperature increases due to Pinatubo aerosols, 19, 207–210, https://doi.org/10.1029/91GL02940, 1992.

Lacis, A., Hansen, J., and Sato, M.: Climate forcing by stratospheric aerosols, Geophys. Res. Lett., 19, 1607–1610, https://doi.org/10.1029/92GL01620, 1992.

Larrasoaña, J. C., Roberts, A. P., and Rohling, E. J.: Dynamics of Green Sahara Periods and Their Role in Hominin Evolution, PLOS ONE, 8, e76514, https://doi.org/10.1371/journal.pone.0076514, 2013.

LeGrande, A. N., Tsigaridis, K., and Bauer, S. E.: Role of atmospheric chemistry in the climate impacts of stratospheric volcanic injections, Nature Geosci, 9, 652–655, https://doi.org/10.1038/ngeo2771, 2016.

Liu, F., Chai, J., Wang, B., Liu, J., Zhang, X., and Wang, Z.: Global monsoon precipitation responses to large volcanic eruptions, Sci Rep, 6, 24331, https://doi.org/10.1038/srep24331, 2016.

Ludlow, F., Stine, A. R., Leahy, P., Murphy, E., Mayewski, P., Taylor, D., Killen, J., Baillie, M., Hennessy, M. and Kiely, G. "Medieval Irish Chronicles Reveal Persistent Volcanic Forcing of Severe

Winter Cold Events, 431-1649 CE”, *Environmental Research Letters*, 8 (2), L024035, doi:10.1088/1748-9326/8/2/024035, 2013.

Ludlow, F. & Manning, J. G. in Climate Change and Ancient Societies in Europe and the Near East: Diversity in Collapse and Resilience (eds Erdkamp, P., Manning, J. G. and Verboven K.) 301-320 (Palgrave Macmillan, 2021).

Ludlow, F. & Manning, J. G. in Revolt and resistance in the Ancient Classical World and the Near East: The crucible of empire (eds Collins, J. J. & Manning, J. G.) 154–171 (Brill, 2016)

Ludlow, F. and Travis, C. (2019) “STEAM Approaches to Climate Change, Extreme Weather and Social-Political Conflict”, In: de la Garza, A. & Travis, C. (eds.), The STEAM Revolution: Transdisciplinary Approaches to Science, Technology, Engineering, Arts, Humanities and Mathematics. New York: Springer, 33-65.

Ludlow, F., Kostick, C. and Morris, C. in The Cambridge World History of Genocide (eds Ben Kiernan, Tracy Maria Lemos and Tristan Taylor) (Cambridge University Press, In Press, 2022).

Ludlow, F. and Crampsie, A.: “Climate, Debt and Conflict: Environmental History as a New Direction in Understanding Early Modern Ireland”, In: Sarah Covington, Vincent Carey and Valerie McGowan-Doyle (eds.), *Early Modern Ireland: New Sources, Methods, and Directions*. London: Routledge, 269-300, 2019.

Ljungqvist, F. C., Seim, A. and Huhtamaa, H.: Climate and Society in European History. WIRE’s Climate Change, 12, e691. https://doi.org/10.1002/wcc.691

Manning, J. G. Land and Power in Ptolemaic Egypt: The Structure of Land Tenure (Cambridge University Press, 2003).

Manning, J. G., Ludlow, F., Stine, A. R., Boos, W. R., Sigl, M., and Marlon, J. R.: Volcanic suppression of Nile summer flooding triggers revolt and constrains interstate conflict in ancient Egypt, Nat Commun, 8, 900, https://doi.org/10.1038/s41467-017-00957-y, 2017.

McCormick, M. P., Thomason, L. W., and Trepte, C. R.: Atmospheric effects of the Mt Pinatubo eruption, Nature, 373, 399–404, https://doi.org/10.1038/373399a0, 1995.

McCormick, M. History's changing climate: Climate science, genomics and the emerging consilient approach to interdisciplinary history,” Journal of Interdisciplinary History 42 (2011): 252-73.

McCormick, M. 2013. 'What climate science, Ausonius, Nile floods, rye, and thatch tell us about the environmental history of the Roman Empire', in 61-88.

McCormick, M. Climates of History, Histories of Climate: From History to Archaeoscience, Journal of Interdisciplinary History, 50 (2019): 3–30.

McConnell, J. R., Sigl, M., Plunkett, G., Burke, A., Kim, W. M., Raible, C. C., Wilson, A. I., Manning, J. G., Ludlow, F., Chellman, N. J., Innes, H. M., Yang, Z., Larsen, J. F., Schaefer, J. R., Kipfstuhl, S., Mojtabavi, S., Wilhelms, F., Opel, T., Meyer, H., and Steffensen, J. P.: Extreme climate after massive eruption of Alaska's Okmok volcano in 43 BCE and effects on the late Roman Republic and Ptolemaic Kingdom, Proc Natl Acad Sci USA, 117, 15443–15449, https://doi.org/10.1073/pnas.2002722117, 2020.

McGing, B. C. Revolt Egyptian style: Internal opposition to Ptolemaic rule. Arch. Papyrusforschung 43, 274–277 (1997).

Mikhail, A. 2015. 'Ottoman Iceland: A climate history', *Environmental History* 20: 262–284.

Melesse, A. M. (Ed.): Nile River Basin, Springer Netherlands, Dordrecht, https://doi.org/10.1007/978-94-007-0689-7, 2011.

Myhre, G., D. Shindell, F.-M. Bréon, W. Collins, J. Fuglestvedt, J. Huang, D. Koch, J.-F. Lamarque, D. Lee, B. Mendoza, T. Nakajima, A. Robock, G. Stephens, T. Takemura, and H. Zhang,: Anthropogenic and natural radiative forcing. In *Climate Change 2013: The Physical Science Basis. Contribution of Working Group I to the Fifth Assessment Report of the Intergovernmental Panel on Climate Change*. T.F. Stocker, D. Qin, G.-K. Plattner, M. Tignor, S.K. Allen, J. Doschung, A. Nauels, Y. Xia, V. Bex, and P.M. Midgley, Eds. Cambridge University Press, pp. 659-740, doi:10.1017/CBO9781107415324.018, 2013

Myneni, R. B., Hoffman, S., Knyazikhin, Y., Privette, J. L., Glassy, J., Tian, Y., Wang, Y., Song, X., Zhang, Y., Smith, G. R., Lotsch, A., Friedl, M., Morisette, J. T., Votava, P., Nemani, R. R., and Running, S. W.: Global products of vegetation leaf area and fraction absorbed PAR from year one of MODIS data, Remote Sensing of Environment, 83, 214–231, https://doi.org/10.1016/S0034-4257(02)00074-3, 2002.

Oman, L., Robock, A., Stenchikov, G., Schmidt, G. A., and Ruedy, R.: Climatic response to high-latitude volcanic eruptions, 110, https://doi.org/10.1029/2004JD005487, 2005.

Oman, L., Robock, A., Stenchikov, G. L., Thordarson, T., Koch, D., Shindell, D. T., and Gao, C.: Modeling the distribution of the volcanic aerosol cloud from the 1783–1784 Laki eruption, J. Geophys. Res., 111, D12209, https://doi.org/10.1029/2005JD006899, 2006.

Otterman, J.: Baring High-Albedo Soils by Overgrazing: A Hypothesized Desertification Mechanism, 186, 531–533, https://doi.org/10.1126/science.186.4163.531, 1974.

Otto-Bliesner, B. L., Braconnot, P., Harrison, S. P., Lunt, D. J., Abe-Ouchi, A., Albani, S., Bartlein, P. J., Capron, E., Carlson, A. E., Dutton, A., Fischer, H., Goelzer, H., Govin, A., Haywood, A., Joos, F., LeGrande, A. N., Lipscomb, W. H., Lohmann, G., Mahowald, N., Nehrbass-Ahles, C., Pausata, F. S. R., Peterschmitt, J.-Y., Phipps, S. J., Renssen, H., and Zhang, Q.: The PMIP4 contribution to CMIP6 – Part 2: Two interglacials, scientific objective and experimental design for Holocene and Last Interglacial simulations, 10, 3979–4003, https://doi.org/10.5194/gmd-10-3979-2017, 2017.

PAGES 2k Consortium, Continental-scale temperature variability during the past two millennia, Nature Geoscience, 6, 339-346 2013.

PAGES 2k Consortium, A global database for temperature reconstructions of the Common Era, Scientific Data, 4:170088 | DOI: 10.1038/sdata.2017.88

PAGES Hydro2k Consortium: Comparing proxy and model estimates of hydroclimate variability and change over the Common Era, 13, 1851–1900, https://doi.org/10.5194/cp-13-1851-2017, 2017.

Parker, D. E., Wilson, H., Jones, P. D., Christy, J. R., and Folland, C. K.: The Impact of Mount Pinatubo on World-Wide Temperatures, 16, 487–497, https://doi.org/10.1002/(SICI)1097-0088(199605)16:5<487::AID-JOC39>3.0.CO;2-J, 1996.

Pausata, F. S. R., Chafik, L., Caballero, R., and Battisti, D. S.: Impacts of high-latitude volcanic eruptions on ENSO and AMOC, Proc Natl Acad Sci USA, 112, 13784–13788, https://doi.org/10.1073/pnas.1509153112, 2015.

Pausata, F. S. R., Messori, G., and Zhang, Q.: Impacts of dust reduction on the northward expansion of the African monsoon during the Green Sahara period, Earth and Planetary Science Letters, 434, 298–307, https://doi.org/10.1016/j.epsl.2015.11.049, 2016.

Peterson, L. C., Haug, G. H., Hughen, K. A., and Röhl, U.: Rapid Changes in the Hydrologic Cycle of the Tropical Atlantic During the Last Glacial, https://doi.org/10.1126/science.290.5498.1947, 2000.

Pitari, G. and Mancini, E.: Short-term climatic impact of the 1991 volcanic eruption of Mt. Pinatubo and effects on atmospheric tracers, Nat. Hazards Earth Syst. Sci., 2, 91–108, https://doi.org/10.5194/nhess-2-91-2002, 2002.

Pitari, G., Cionni, I., Di Genova, G., Visioni, D., Gandolfi, I., and Mancini, E.: Impact of Stratospheric Volcanic Aerosols on Age-of-Air and Transport of Long-Lived Species, 7, 149, https://doi.org/10.3390/atmos7110149, 2016.

Rachmayani, R., Prange, M., and Schulz, M.: North African vegetation–precipitation feedback in early and mid-Holocene climate simulations with CCSM3-DGVM, Clim. Past, 11, 175–185, https://doi.org/10.5194/cp-11-175-2015, 2015. https://doi.org/10.5194/cp-11-175-2015, 2015.

Rao, M. P., Cook, B. I., Cook, E. R., D'Arrigo, R. D., Krusic, P. J., Anchukaitis, K. J., LeGrande, A. N., Buckley, B. M., Davi, N. K., Leland, C., and Griffin, K. L.: European and Mediterranean hydroclimate responses to tropical volcanic forcing over the last millennium, 44, 5104–5112, https://doi.org/10.1002/2017GL073057, 2017.

Read, W. G., Froidevaux, L., and Waters, J. W.: Microwave limb sounder measurement of stratospheric SO2 from the Mt. Pinatubo Volcano, 20, 1299–1302, https://doi.org/10.1029/93GL00831, 1993.

Robock, A.: Volcanic eruptions and climate, 38, 191–219, https://doi.org/10.1029/1998RG000054, 2000.

Robock, A. and Mao, J.: Winter warming from large volcanic eruptions, Geophys. Res. Lett., 19, 2405–2408, https://doi.org/10.1029/92GL02627, 1992.

Robock, A. and Liu, Y.: The Volcanic Signal in Goddard Institute for Space Studies Three-Dimensional Model Simulations, 7, 44–55, https://doi.org/10.1175/1520-0442(1994)007<0044:TVSIGI>2.0.CO;2, 1994.

Robock, A. and Mao, J.: The Volcanic Signal in Surface Temperature Observations, 8, 1086–1103, https://doi.org/10.1175/1520-0442(1995)008<1086:TVSIST>2.0.CO;2, 1995.

Roger S. Bagnall and Peter Derow, *Historical Sources in Translation. The Hellenistic Period*. New Edition, Blackwell, 2004.

Roller, D. W. Cleaopatra: A Biography (Oxford University Press, 2010).

Sabzevari, A. A., Zarenistanak, M., Tabari, H., and Moghimi, S.: Evaluation of precipitation and river discharge variations over southwestern Iran during recent decades, J Earth Syst Sci, 124, 335–352, https://doi.org/10.1007/s12040-015-0549-x, 2015.

Russell, P. B., Livingston, J. M., Pueschel, R. F., Bauman, J. J., Pollack, J. B., Brooks, S. L., Hamill, P., Thomason, L. W., Stowe, L. L., Deshler, T., Dutton, E. G., and Bergstrom, R. W.: Global to microscale evolution of the Pinatubo volcanic aerosol derived from diverse measurements and analyses, 101, 18745–18763, https://doi.org/10.1029/96JD01162, 1996.

Schmidt, A., Carslaw, K. S., Mann, G. W., Wilson, M., Breider, T. J., Pickering, S. J., and Thordarson, T.: The impact of the 1783–1784 AD Laki eruption on global aerosol formation processes and cloud condensation nuclei, 10, 6025–6041, https://doi.org/10.5194/acp-10-6025-2010, 2010.

Schmidt, G. A., Ruedy, R., Hansen, J. E., Aleinov, I., Bell, N., Bauer, M., Bauer, S., Cairns, B., Canuto, V., Cheng, Y., Del Genio, A., Faluvegi, G., Friend, A. D., Hall, T. M., Hu, Y., Kelley, M., Kiang, N. Y., Koch, D., Lacis, A. A., Lerner, J., Lo, K. K., Miller, R. L., Nazarenko, L., Oinas, V., Perlwitz, J., Perlwitz, J., Rind, D., Romanou, A., Russell, G. L., Sato, M., Shindell, D. T., Stone, P. H., Sun, S., Tausnev, N., Thresher, D., and Yao, M.-S.: Present-Day Atmospheric Simulations Using GISS ModelE: Comparison to In Situ, Satellite, and Reanalysis Data, 19, 153–192, https://doi.org/10.1175/JCLI3612.1, 2006.

Schmidt, G. A., Jungclaus, J. H., Ammann, C. M., Bard, E., Braconnot, P., Crowley, T. J., Delaygue, G., Joos, F., Krivova, N. A., Muscheler, R., Otto-Bliesner, B. L., Pongratz, J., Shindell, D. T., Solanki, S. K., Steinhilber, F., and Vieira, L. E. A.: Climate forcing reconstructions for use in PMIP simulations of the last millennium (v1.0), Geosci. Model Dev., 4, 33–45, https://doi.org/10.5194/gmd-4-33-2011, 2011.

Schmidt, G. A., Kelley, M., Nazarenko, L., Ruedy, R., Russell, G. L., Aleinov, I., Bauer, M., Bauer, S. E., Bhat, M. K., Bleck, R., Canuto, V., Chen, Y.-H., Cheng, Y., Clune, T. L., Del Genio, A., de Fainchtein, R., Faluvegi, G., Hansen, J. E., Healy, R. J., Kiang, N. Y., Koch, D., Lacis, A. A., LeGrande, A. N., Lerner, J., Lo, K. K., Matthews, E. E., Menon, S., Miller, R. L., Oinas, V., Oloso, A. O., Perlwitz, J. P., Puma, M. J., Putman, W. M., Rind, D., Romanou, A., Sato, M., Shindell, D. T., Sun, S., Syed, R. A., Tausnev, N., Tsigaridis, K., Unger, N., Voulgarakis, A., Yao, M.-S., and Zhang, J.: Configuration and assessment of the GISS ModelE2 contributions to the CMIP5 archive: GISS MODEL-E2 CMIP5 SIMULATIONS, J. Adv. Model. Earth Syst., 6, 141–184, https://doi.org/10.1002/2013MS000265, 2014.

Said, R. 1993. The River Nile: Geology, Hydrology and Utilization. Oxford.

Schneider, D. P., Ammann, C. M., Otto-Bliesner, B. L., and Kaufman, D. S.: Climate response to large, high-latitude and low-latitude volcanic eruptions in the Community Climate System Model, 114, https://doi.org/10.1029/2008JD011222, 2009.

Schneider A. W. and Adali, S.F. : ''No Harvest was Reaped': Demographic and Climatic Factors in the Decline of the Neo-Assyrian Empire', *Climatic Change* 127, pp.435-446, 2014.

Schnetzler, C. C., Krueger, A. J., Bluth, G. S., Sprod, I. E., and Walter, L. S.: Comment on the Paper "The atmospheric SO2 budget for Pinatubo derived from NOAA-11 SBUV/2 spectral data" by R. D. McPeters, 22, 315–316, https://doi.org/10.1029/94GL02406, 1995.

Segele, Z. T., Lamb, P. J., and Leslie, L. M.: Large-scale atmospheric circulation and global sea surface temperature associations with Horn of Africa June–September rainfall, 29, 1075–1100, https://doi.org/10.1002/joc.1751, 2009.

Shindell, D. T.: Dynamic winter climate response to large tropical volcanic eruptions since 1600, J. Geophys. Res., 109, D05104, https://doi.org/10.1029/2003JD004151, 2004.

Shindell, D. T., Faluvegi, G., Unger, N., Aguilar, E., Schmidt, G. A., Koch, D. M., Bauer, S. E., and Miller, R. L.: Simulations of preindustrial, present-day, and 2100 conditions in the NASA GISS composition and climate model G-PUCCINI, 6, 4427–4459, https://doi.org/10.5194/acp-6-4427-2006, 2006.

Sigl, M., Winstrup, M., McConnell, J. R., Welten, K. C., Plunkett, G., Ludlow, F., Büntgen, U., Caffee, M., Chellman, N., Dahl-Jensen, D., Fischer, H., Kipfstuhl, S., Kostick, C., Maselli, O. J., Mekhaldi, F., Mulvaney, R., Muscheler, R., Pasteris, D. R., Pilcher, J. R., Salzer, M., Schüpbach, S., Steffensen, J. P., Vinther, B. M., and Woodruff, T. E.: Timing and climate forcing of volcanic eruptions for the past 2,500 years, Nature, 523, 543–549, https://doi.org/10.1038/nature14565, 2015.

Simard, M., Pinto, N., Fisher, J. B., and Baccini, A.: Mapping forest canopy height globally with spaceborne lidar, 116, https://doi.org/10.1029/2011JG001708, 2011.

Singh, R. and AchutaRao, K.: Quantifying uncertainty in twenty-first century climate change over India, Clim Dyn, 52, 3905–3928, https://doi.org/10.1007/s00382-018-4361-6, 2019.

Singh, R., LeGrande, A. N., and Tsigaridis, K.: Influence of regional anthropogenic changes over Nile region on the climate system during the late Holocene (~2500 years before present), EGU General Assembly 2020, Online, 4–8 May 2020, EGU2020-12338, https://doi.org/10.5194/egusphere-egu2020-12338, 2020.

Staunton-Sykes, J., Aubry, T. J., Shin, Y. M., Weber, J., Marshall, L. R., Luke Abraham, N., Archibald, A., and Schmidt, A.: Co-emission of volcanic sulfur and halogens amplifies volcanic effective radiative forcing, 21, 9009–9029, https://doi.org/10.5194/acp-21-9009-2021, 2021.

Solway, J. S. :'Drought as a Revelatory Crisis: An Exploration of Shifting Entitlements and Hierarchies in the Kalahari, Botswana', *Development and Change* 25, pp.471-495, 1994.

Stenchikov, G.: Chapter 26 - The Role of Volcanic Activity in Climate and Global Change, in: Climate Change (Second Edition), edited by: Letcher, T. M., Elsevier, Boston, 419–447, https://doi.org/10.1016/B978-0-444-63524-2.00026-9, 2016.

Stoffel, M., Corona, C., Ludlow, F., Sigl, M., Huhtamaa, H., Garnier, E., Helama, S., Guillet, S., Crampsie, A., Kleemann, K., Camenisch, C., McConnell, J. and Gao, C. (In Review, 2022), "Climatic, Weather and Socio-Economic Conditions Corresponding with the mid-17th Century Eruption Cluster", *Climate of the Past.*

Swingedouw, D., Mignot, J., Ortega, P., Khodri, M., Menegoz, M., Cassou, C., and Hanquiez, V.: Impact of explosive volcanic eruptions on the main climate variability modes, Global and Planetary Change, 150, 24–45, https://doi.org/10.1016/j.gloplacha.2017.01.006, 2017.

Sołtysiak, A. : 'Drought and the Fall of Assyria: Quite Another Story', *Climatic Change* 136, 2016, pp.389-394, 2016.

Tardif, R., Hakim, G.J., Perkins, W.A., Horlick, K.A., Erb, M.P., Emile-Geay, J., Anderson, D.M., Steig, E.J. & Noone, D. (2019). Last Millennium Reanalysis with an Expanded Proxy Database and Seasonal Proxy Modeling, *Climate of the Past*, 15, pp. 1251-1273.

Thordarson, T.: Atmospheric and environmental effects of the 1783–1784 Laki eruption: A review and reassessment, J. Geophys. Res., 108, 4011, https://doi.org/10.1029/2001JD002042, 2003.

Tierney, J. E., Pausata, F. S. R., and deMenocal, P. B.: Rainfall regimes of the Green Sahara, https://doi.org/10.1126/sciadv.1601503, 2017.

Timmreck, C., Lorenz, S. J., Crowley, T. J., Kinne, S., Raddatz, T. J., Thomas, M. A., and Jungclaus, J. H.: Limited temperature response to the very large AD 1258 volcanic eruption, Geophys. Res. Lett., 36, L21708, https://doi.org/10.1029/2009GL040083, 2009.

Timmreck, C., Graf, H.-F., Lorenz, S. J., Niemeier, U., Zanchettin, D., Matei, D., Jungclaus, J. H., and Crowley, T. J.: Aerosol size confines climate response to volcanic super-eruptions, 37, https://doi.org/10.1029/2010GL045464, 2010.

Timmreck, C.: Modeling the climatic effects of large explosive volcanic eruptions, 3, 545–564, https://doi.org/10.1002/wcc.192, 2012.

Tiwari, S., Ramos, R., Pausata, F. S. R., LeGrande, A. N., Griffiths, M. L., Beltrami, H., Chandan, D., de Vernal, A., Litchmore, D., Peltier, R., and Tabor, C. R.: Model performance in simulating the mid-Holocene Green Sahara, EGU General Assembly 2022, Vienna, Austria, 23–27 May 2022, EGU22-3233, https://doi.org/10.5194/egusphere-egu22-3233, 2022

Toohey, M., Krüger, K., Niemeier, U., and Timmreck, C.: The influence of eruption season on the global aerosol evolution and radiative impact of tropical volcanic eruptions, Atmos. Chem. Phys., 11, 12351–12367, https://doi.org/10.5194/acp-11-12351-2011, 2011.

Toohey, M. and Sigl, M.: Volcanic stratospheric sulfur injections and aerosol optical depth from 500 BCE to 1900 CE, 9, 809–831, https://doi.org/10.5194/essd-9-809-2017, 2017.

Toohey, M., Krüger, K., Sigl, M., Stordal, F., and Svensen, H.: Climatic and societal impacts of a volcanic double event at the dawn of the Middle Ages, Climatic Change, 136, 401–412, https://doi.org/10.1007/s10584-016-1648-7, 2016.

Toohey, M., Krüger, K., Schmidt, H., Timmreck, C., Sigl, M., Stoffel, M., and Wilson, R.: Disproportionately strong climate forcing from extratropical explosive volcanic eruptions, 12, 100–107, https://doi.org/10.1038/s41561-018-0286-2, 2019.

Trepte, C. R. and Hitchman, M. H.: Tropical stratospheric circulation deduced from satellite aerosol data, Nature, 355, 626–628, https://doi.org/10.1038/355626a0, 1992.

Travis, C., Holm, P., Ludlow, F., Kostick, C., McGovern, R. and Nicholls, J. (2022) “Cowboys, Cod, Climate and Conflict: Navigations in the Digital Environmental Humanities”, In: Travis, C., Legg, R., Bergmann, L., Crampsie, A. and Dixon, D. (eds.), *Routledge Handbook of the Digital Environmental Humanities*. London: Routledge, 17-39.

Trenberth, K. E. and Dai, A.: Effects of Mount Pinatubo volcanic eruption on the hydrological cycle as an analog of geoengineering: PINATUBO AND THE HYDROLOGICAL CYCLE, Geophys. Res. Lett., 34, https://doi.org/10.1029/2007GL030524, 2007.Vashisht, A., Zaitchik, B., and Gnanadesikan, A.: ENSO Teleconnection to Eastern African Summer Rainfall in Global Climate Models: Role of the Tropical Easterly Jet, 34, 293–312, https://doi.org/10.1175/JCLI-D-20-0222.1, 2021.

Vashisht, A., Zaitchik, B., and Gnanadesikan, A.: ENSO Teleconnection to Eastern African Summer Rainfall in Global Climate Models: Role of the Tropical Easterly Jet, 34, 293–312, https://doi.org/10.1175/JCLI-D-20-0222.1, 2021.

van Bavel, B.J.P., Curtis, D.R., Hannaford, M.J., Moatsos, M., Roosen, J., and Soens, T.: Climate and society in long-term perspective: Opportunities and pitfalls in the use of historical datasets, Wires Clim. Change, 10(6), e611, doi: 10.1002/wcc.611, 2019.

Vehkamäki, H., Kulmala, M., Napari, I., Lehtinen, K. E. J., Timmreck, C., Noppel, M., and Laaksonen, A.: An improved parameterization for sulfuric acid–water nucleation rates for tropospheric and stratospheric conditions, 107, AAC 3-1-AAC 3-10, https://doi.org/10.1029/2002JD002184, 2002.

Veïsse, A.-E.: Les révoltes égyptiennes: recherches sur les troubles intérieurs en Égypte du règne de Ptolémée III à la conquête romaine, Peeters, Leuven; Paris; Dudley, MA, 2004.

Vörösmarty, CJ; Fekete, BM; Tucker, BA (1998): Global River Discharge, 1807-1991, V. 1.1 (RivDIS). Data set. Available on-line [http://www.daac.ornl.gov] from Oak Ridge National Laboratory Distributed Active Archive Center, Oak Ridge, Tennessee, U.S.A.

Wahl, E. R., Diaz, H. F., Smerdon, J. E., and Ammann, C. M.: Late winter temperature response to large tropical volcanic eruptions in temperate western North America: Relationship to ENSO phases, Global and Planetary Change, 122, 238–250, https://doi.org/10.1016/j.gloplacha.2014.08.005, 2014.

Wolfe, E. W., and Hoblitt R. P.: Overview of the eruptions, in Fire and Mud: Eruptions and lahars of the Moun Pinatubo, Philippines, edited by Newhall C.G. and Punongbayan, pp. 415-433, Univ of Wash. Press, Seattle.

White, S. and Pei, Q. (2020). Attribution of historical societal impacts and adaptations to climate and extreme events: Integrating quantitative and qualitative perspectives. Past Global Changes Magazine, 28(2), 44-45.

Xian, P. and Miller, R. L.: Abrupt Seasonal Migration of the ITCZ into the Summer Hemisphere, 65, 1878–1895, https://doi.org/10.1175/2007JAS2367.1, 2008.

Zanchettin, D., Bothe, O., Graf, H. F., Lorenz, S. J., Luterbacher, J., Timmreck, C., and Jungclaus, J. H.: Background conditions influence the decadal climate response to strong volcanic eruptions, 118, 4090–4106, https://doi.org/10.1002/jgrd.50229, 2013.

Zanchettin, D., Timmreck, C., Khodri, M., Schmidt, A., Toohey, M., Abe, M., Bekki, S., Cole, J., Fang, S.-W., Feng, W., Hegerl, G., Johnson, B., Lebas, N., LeGrande, A. N., Mann, G. W., Marshall, L., Rieger, L., Robock, A., Rubinetti, S., Tsigaridis, K., and Weierbach, H.: Effects of forcing differences and initial conditions on inter-model agreement in the VolMIP volc-pinatubo-full experiment, 1–39, https://doi.org/10.5194/gmd-2021-372, 2021.

Investigating hydroclimatic impacts of the 168-158 BCE volcanic quartet and their relevance to the Nile River basin and Egyptian history

Ram Singh[1,2], Kostas Tsigaridis[1,2], Allegra N. LeGrande[2,1], Francis Ludlow[3], Joseph G Manning[4]

[1] Center for Climate Systems Research, Columbia University, New York
[2] NASA Goddard Institute for Space Studies, New York, NY-10025
[3] Department of History, School of Histories and Humanities, Trinity College, Dublin 2, Ireland
[4] Departments of History and Classics, Yale University, New Haven, CT 06520, USA

Correspondence to: Ram Singh (rs4068@columbia.edu)

Supplementary information

S1.1 Introduction (Historical Context)

Important questions remain, however, in particular on the role of hydroclimatic shocks in the longer-term declining stability of the state and its ability to project power across the eastern Mediterranean. Repeated revolt in the third to first centuries BCE speaks to persistent vulnerability, yet despite experiencing the hydroclimatic effects of multiple eruptions (including those with a greater climate forcing potential than has been experienced in the twentieth and twenty-first centuries (Sigl et al., 2015) and multiple such revolts, the dynasty persisted for almost three centuries, simultaneously suggesting a considerable level of resilience. It is conspicuous, however, that the dynasty ultimately ended (with Cleopatra's defeat by Rome at the naval battle of Actium in 31 BCE and her suicide in 30 BCE) in a decade that followed one of the largest explosive eruptions of the last 2,500 years in terms of climate forcing potential (based upon polar ice-core sulfate deposition levels), that of Okmok (Alaska) in early 43 BCE (McConnell et al., 2020). This itself followed a smaller but notable (likely extratropical NH eruption) in 46 BCE

(McConnell et al., 2020). Egypt in the 40s BCE had, perhaps unsurprisingly therefore, experienced repeated Nile failure, famine, plague, inflation, administrative corruption, rural depopulation, migration, and land abandonment (Hölbl, 2001; Roller, 2010). It is notable though that there is no convincingly documented revolt, perhaps owing to Cleopatra's abilities as a leader and interventions in grain distribution to prevent starvation of the population. The stresses of the 40s BCE may still, however, be credibly posited as weakening Egypt's hand against Rome as it became entangled in the complex political and military developments of this major moment in world history, as Rome transitioned from its republic to imperial form (Manning et al., 2017; McConnell et al., 2020; Ludlow and Manning, 2021).

Here clearly, as at any other time, the societal impact of a given hydroclimatic shock will be mediated by the prevailing historical context, but this does not mean all hydroclimatic shocks are of equal potential impact. Thus, regarding the association between explosive volcanism and Chinese dynastic collapse over the Common Era, the societal efficacy of volcanic climate forcing was observed to depend not only on levels of pre-existing or contemporaneous societal stress or instability (i.e., the historical context), but also on the magnitude of the climate forcing itself (Gao et al., 2021). Ice-core data suggest that the sequence of approximately 24 tropical and extratropical NH eruptions experienced by Ptolemaic Egypt varied in their climate forcing potential and were not distributed evenly in time (Sigl et al., 2015; Manning et al., 2017). Clusters of historical eruptions have at other times been examined for their potentially severe climatic and societal impacts (e.g., Toohey et al., 2016; Guillet et al., 2020; Campbell and Ludlow, 2020; Stoffel et al., 2022) and such an investigation can make a meaningful contribution to our understanding of the role of explosive volcanism in the history of Ptolemaic Egypt

Table TS1: Table showing the order and specification of the 2.5ka control run. The latest 100 years of the 2.5ka (GHG+ORB+VEG) run are used to represent the base climate for the 2.5ka period. NINT: Non-INTeractive version, MATRIX: Multiconfiguration Aerosol TRacker of mIXing state.

order of control runs and volcanic experiments				
ModelE (NINT) 2.5ka control run (1000 years)	ModelE (MATRIX) 2.5ka control run (100 years)	ModelE (MATRIX) 2.5ka control run (70 years) 2.5ka (GHG+ORB)	ModelE (MATRIX) 2.5ka control run (130 years) 2.5ka (GHG+ORB+VEG)	ModelE (MATRIX) 10 ensemble members (Initialized using restart files at 10 years gap) 2.5ka (GHG+ORB+VEG)
Orbital forcing (2.5ka), Greenhouse gases (2.5ka), Vegetations (PI)	Orbital forcing (2.5ka), Greenhouse gases (2.5ka), Vegetations (PI)	Orbital forcing (2.5ka), Greenhouse gases (2.5ka), Vegetations (PI) Retuned Dust Parameters	Orbital forcing (2.5ka), Greenhouse gases (2.5ka), PMIP4 Vegetations (Interpolated for 2.5ka) Retuned Dust Parameters	Orbital forcing (2.5ka), Greenhouse gases (2.5ka), PMIP4 Vegetations (Interpolated for 2.5ka) Retuned Dust Parameters Volcanic SO_2 injection for 4 eruptions during 158-168 BCE (Sigl et al., 2015)

Deleted: *<object>*

Inserted Cells

Inserted Cells

Deleted: PI)

Fig S1: Spatial representation of changes in major vegetation plant function types (PFTs) under the PMIP4 sensitivity protocol (Otto-Bliesner et al., 2017) after interpolating for the 2.5ka period. Top row shows arid shrub and boreal forest changes, bottom row show C3 and C4 grasses.

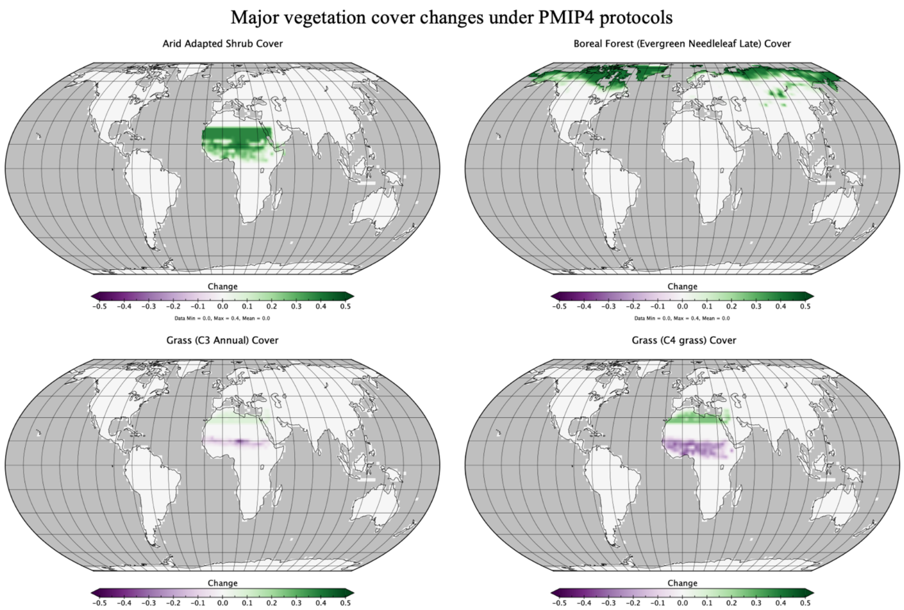

Fig S2. Timeseries of annual global mean surface air temperature (top) and precipitation (bottom) for the 2.5ka control run with (green) and without (red) the altered vegetation (see text). Vertical blue lines show the starting points of all 10 ensemble members.

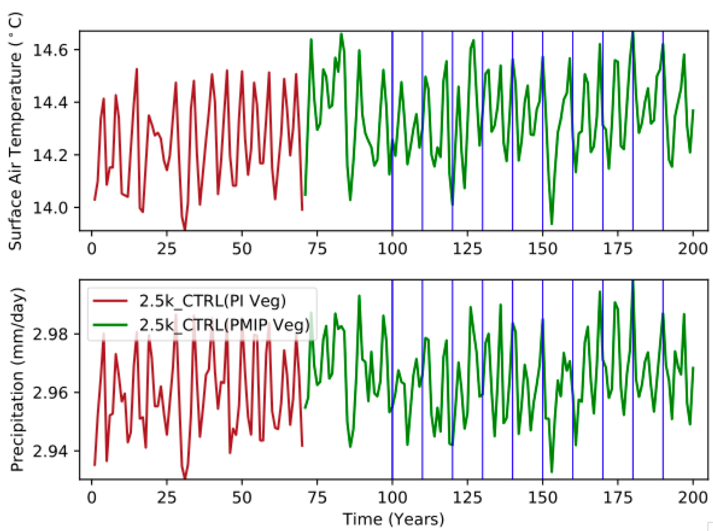

Fig S3. Geographical positions of all 4 volcanic eruptions during the study period are distinguished by different colours. First eruption (E1, Red) erupted during 168 BCE, second (E2, Blue) during 164 BCE, third (E3, Magenta) during 161 BCE and fourth (E4, Orange) erupted during 158 BCE. Spatial box (with caption Nile H) shows the spatial extent of the region considered as the Nile River watershed (discussed in Fig12, main text).

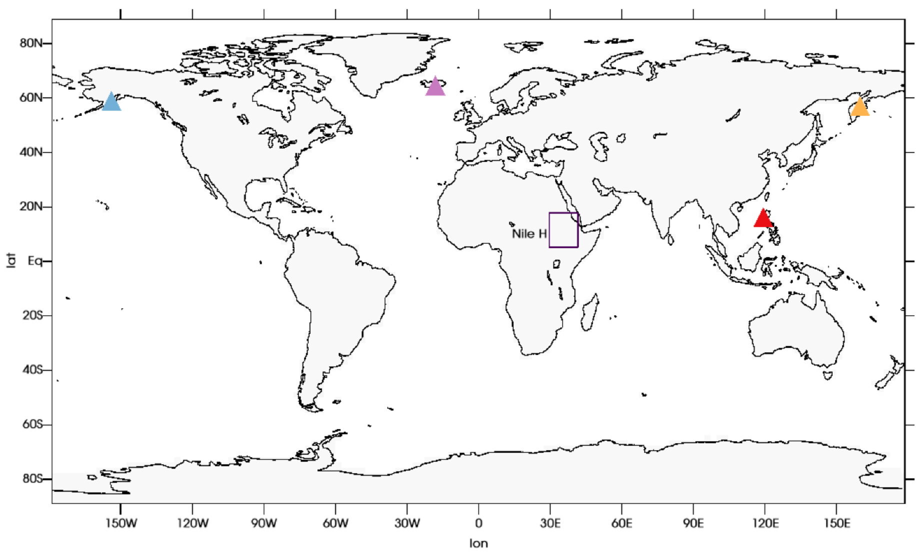

Fig S4: Globally averaged change in sea surface temperature (top panel), surface air temperature over land (middle panel) and over ocean (bottom panel) for each month for the entire simulation period. The light-colored solid lines represent individual ensemble members, and the solid dark colors show the ensemble means. The green vertical dashed lines show the dating of the four eruptions (E1-E4).

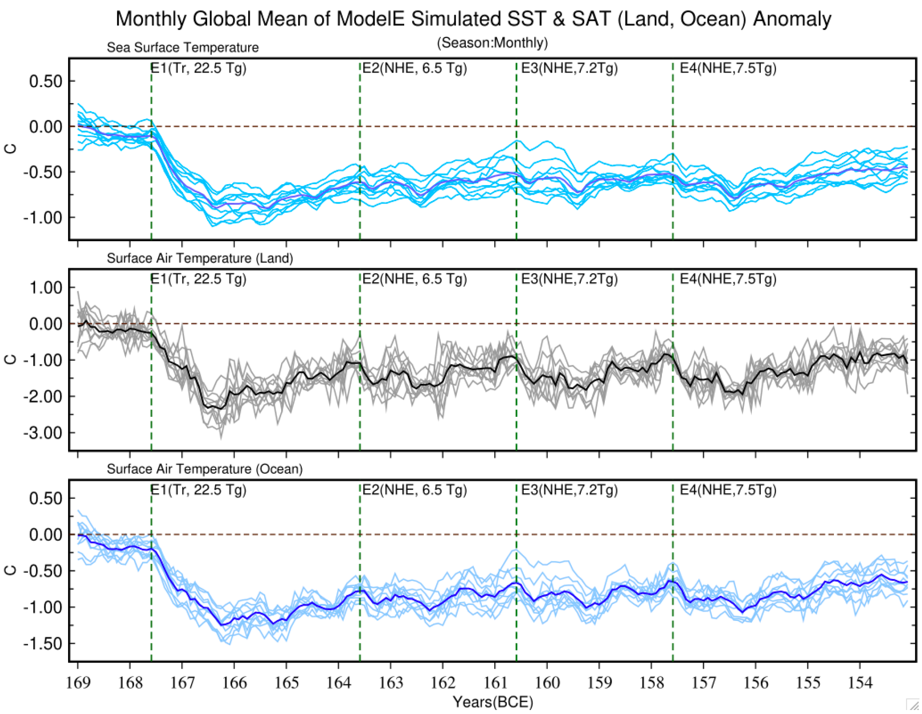

Fig S5. Vertical profile of extinction (A) and methane (CH_4; B) change following the volcanic eruptions. Vertical black line represents the timing of each eruption.

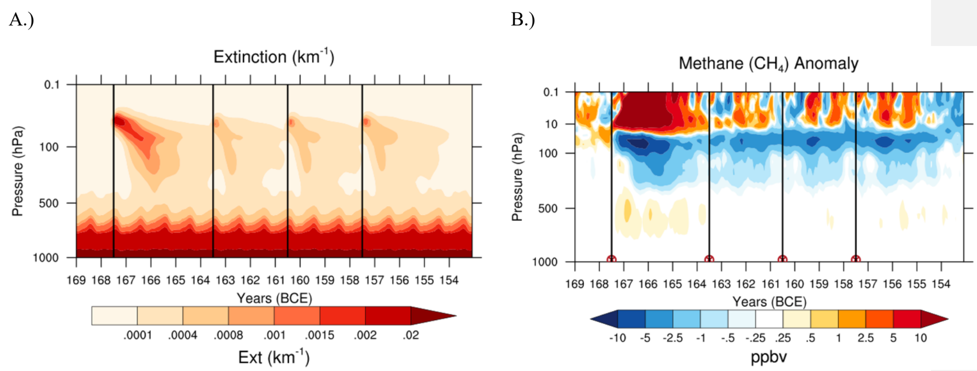

Fig S6. Spatial pattern of seasonal mean surface temperature response (˚C) for the four seasons following the first eruption E1. Column 1 show the JJA (June, July August) and SON (September, October, November) for the year of eruption. Column 2 shows the DJF (December, January, February) of the eruption year and first following year, and the MAM (March, April, May) of the first following year. Stippling marks the regions where differences are not significant.

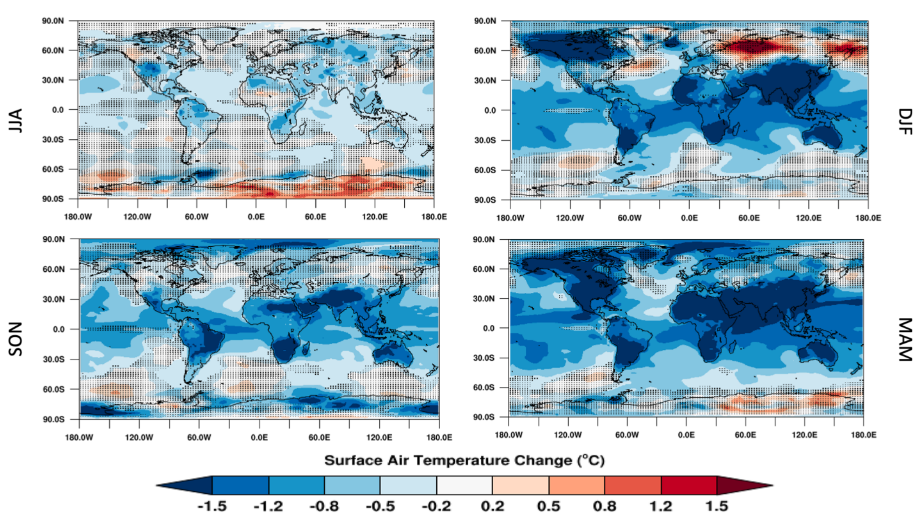

Fig S7. Total cloud cover change during the monsoon season (JJAS) for 3 consecutive years after each eruption (columns) over the North African continent. The blue line demarks the present-day Nile River basin boundary, which is broadly similar to the river extent approximately 2.5ka years ago. The red stippling indicates regions over which change in rainfall is not significant at the 95% confidence level.